

Potent and selective SETDB1 covalent negative allosteric modulator reduces methyltransferase activity in cells

Received: 22 September 2024

Accepted: 4 February 2025

Published online: 24 February 2025



Mélanie Uguen¹, Devan J. Shell¹, Madhushika Silva², Yu Deng^{3,4}, Fengling Li², Magdalena M. Szewczyk², Ka Yang⁵, Yani Zhao¹, Michael A. Stashko¹, Jacqueline L. Norris-Drouin¹, Jarod M. Waybright^{1,7}, Serap Beldar², Justin M. Rectenwald¹, Angie L. Mordant⁶, Thomas S. Webb⁶, Laura E. Herring⁶, Cheryl H. Arrowsmith², Suzanne Ackloo², Steven P. Gygi⁵, Robert K. McGinty^{1,3,4}, Dalia Barsyte-Lovejoy², Pengda Liu^{3,4}, Levon Halabelian², Lindsey I. James^{1,3}, Kenneth H. Pearce^{1,3} & Stephen V. Frye^{1,3} ✉

A promising drug target, SETDB1, is a dual methyl-lysine (Kme) reader and methyltransferase implicated in cancer and neurodegenerative disease progression. To help understand the role of the triple Tudor domain (3TD) of SETDB1, its Kme reader, we first identify a low micromolar potency small molecule ligand, UNC6535, which occupies simultaneously both the TD2 and TD3 reader binding sites. Further optimization leads to the discovery of UNC10013, a covalent 3TD ligand targeting Cys385 of SETDB1. UNC10013 is potent with a k_{inact}/K_i of $1.0 \times 10^6 \text{ M}^{-1}\text{s}^{-1}$ and demonstrates proteome-wide selectivity. In cells, negative allosteric modulation of SETDB1-mediated Akt methylation occurs after treatment with UNC10013. Therefore, UNC10013 is a potent, selective, and cell-active covalent ligand for the 3TD of SETDB1, demonstrating negative allosteric modulator properties and making it a promising tool to study the biological role of SETDB1 in disease progression.

Histone lysine methylation is a key post-translational modification that regulates differentiation, development, and gene transcription. Specific lysine methylation motifs on histones are installed by lysine methyltransferases, removed by lysine demethylases, and read by methyl lysine (Kme) readers^{1,2}. Kme reader proteins bind to histones when they exhibit the required methylation levels at a specific lysine residue³. This binding event triggers downstream effects which influence gene expression or repression. Aberrant activity and overexpression of Kme readers correlate with disease progression, notably

in cancer, and although the structural basis for Kme reader binding to histones is generally well understood, the resulting signaling cascades are less well-studied and would benefit from the development of high-quality chemical probes^{4,5}.

SET domain bifurcated 1 (SETDB1) belongs to the Kme reader protein family as it contains three different Tudor domains, forming the triple Tudor domain (3TD), a binding domain for the histone 3 tail when lysine 9 is di- or tri- methylated and lysine 14 is acetylated (H3K9Me2/3K14Ac). The dimethylated lysine of H3K9Me2K14Ac

¹UNC Eshelman School of Pharmacy, Center for Integrative Chemical Biology and Drug Discovery, Chemical Biology and Medicinal Chemistry, University of North Carolina at Chapel Hill, Chapel Hill, NC, USA. ²University of Toronto, Toronto, ON, Canada. ³Lineberger Comprehensive Cancer Center, University of North Carolina at Chapel Hill School of Medicine, Chapel Hill, NC, USA. ⁴Department of Biochemistry and Biophysics, The University of North Carolina at Chapel Hill, Chapel Hill, NC, USA. ⁵Department of Cell Biology, Harvard Medical School, Boston, MA, USA. ⁶UNC Metabolomics and Proteomics Core Facility, Department of Pharmacology, University of North Carolina at Chapel Hill, Chapel Hill, NC, USA. ⁷Present address: Design Therapeutics, Carlsbad, CA, USA.

✉ e-mail: svfrye@email.unc.edu

occupies the aromatic cage of TD3, but when it is trimethylated it can also bind to the aromatic cage of the TD2⁶. Importantly, the biological consequences of these two binding events are not fully understood.

In addition to its 3TD reader domain, SETDB1 also contains a methyltransferase domain which catalyzes the di- and tri-methylation of lysine 9 of the histone 3 tail as well as the methylation of non-histone proteins such as Akt1, p53 and MCT1^{7–11}. It is currently unclear how the 3TD and the SET domain of SETDB1 interact or if they cooperate in modulating the same signaling cascade.

Recently, a reversible small molecule ligand that binds the Tudor domain 2 (TD2) and the interface of TD2-TD3 of SETDB1, (*R,R*)-59, and can displace a H3K9Me2 peptide from the 3TD was reported¹². Interestingly, we find that this compound promotes the SETDB1-mediated methylation of Akt1, making it a positive allosteric modulator for SETDB1; suggestive of cross-talk between the 3TD and SET domains¹³.

Here, we disclose the identification of UNC6535, a small molecule ligand that reversibly binds both the TD2 and TD3 aromatic cages. Based on the crystal structure of UNC6535, a series of covalent analogs targeting Cys385 are designed and characterized. Among them, UNC10013 is a potent and selective covalent ligand for the 3TD, with a k_{inact}/K_i of $1.0 \times 10^6 \text{ M}^{-1}\text{s}^{-1}$, demonstrating proteome-wide selectivity, and which showed no significant direct inhibition of the methyltransferase activity of SETDB1 in vitro. However, in cells, UNC10013 decreases the ability of SETDB1 to methylate the Akt kinase in a dose-dependent manner through an allosteric mechanism. Overall, this study successfully identifies a potent and selective negative allosteric modulator for SETDB1-mediated Akt methylation.

Results

Identification of reversible ligand UNC6535

Screening of an in-house Kme reader-targeted library of small molecules by a time-resolved fluorescence resonance energy transfer (TR-FRET) detection of the displacement of an H3K9Me2K14Ac peptide¹³ revealed UNC6535 as a 3TD ligand with an IC_{50} of $3.4 \pm 0.7 \mu\text{M}$ (Fig. 1a). An orthogonal isothermal titration calorimetry assay confirmed that UNC6535 binds SETDB1 3TD with a K_d of $4.2 \pm 1.1 \mu\text{M}$ (Supplementary Fig. 1). UNC6535 also demonstrated the ability to weakly inhibit SETDB1 methyltransferase activity in an in vitro radiometric methyltransferase assay¹³ with an IC_{50} of $84 \pm 13 \mu\text{M}$ for the full-length protein (SETDB1-FL, aa 1–1291) and $30 \pm 3 \mu\text{M}$ on a SETDB1 construct (SETDB1-S, aa 570–1291) that does not contain the 3TD (Supplementary Fig. 2). A fluorescence polarization (FP) displacement assay showed an IC_{50} of $8.6 \pm 0.9 \mu\text{M}$ for the displacement of FITC-H3 (1–25) from SETDB1-S by UNC6535 (Supplementary Fig. 3). This shows that UNC6535 lacks selectivity for the 3TD and may also interact with the SET domain.

A crystal structure of UNC6535 bound to the 3TD of SETDB1 shows the formation of cation- π interactions with the aromatic cages of TD2 and TD3 (Fig. 1b). The dimethylamine chain from position 2 of the quinazoline forms cation- π interactions with Tyr268, Tyr277, and Phe297 and a salt bridge with Asp299 from the TD2 aromatic cage. The second dimethylamine chain forms cation- π interactions with Trp358, Trp363, and Phe379 of the TD3 aromatic cage. Other favorable interactions include π - π stacking between the quinazoline core and Tyr301 and a hydrogen bond between the nitrogen atom at position 1 of the quinazoline and Asp270. Interestingly, UNC6535 shares the ability to

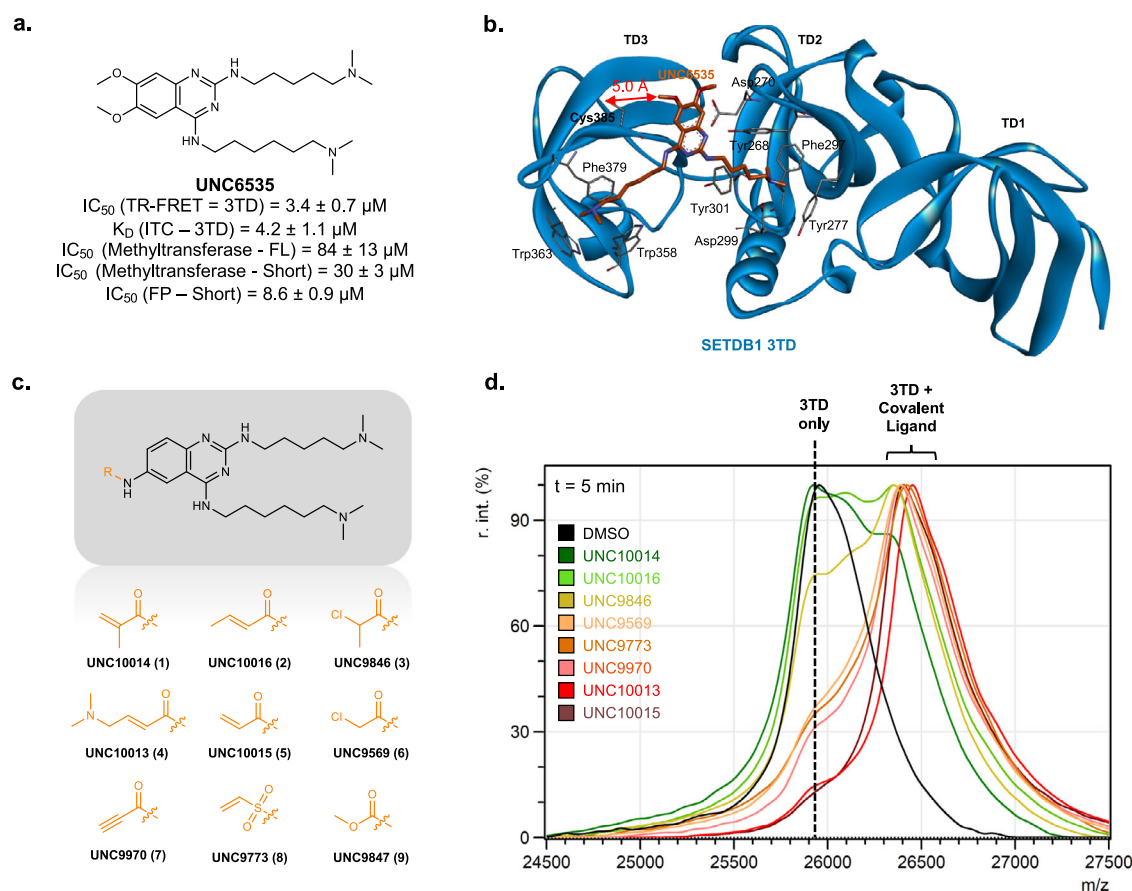


Fig. 1 | Structure-based design of UNC6535 analogs aimed at covalently binding to the 3TD. a Structure and characterization of UNC6535. Reported IC_{50} and K_d values are the average of two (ITC – $n = 2$) or three (others – $n = 3$) independent biological replicates \pm s.d. Source data are provided as a Source Data file. **b** Crystal structure of UNC6535 bound to SETDB1 3TD (PDB: 8G5E). **c** Structure of nine

covalent analogs of UNC6535 1–9 that were synthesized and tested. **d** Representative MALDI-TOF qualitative evaluation of the ability of 1–9 to covalently modify SETDB1 3TD (1:1 ratio) after 5 min incubation on ice. TR-FRET time-resolved fluorescence resonance energy transfer, ITC isothermal titration calorimetry, FP fluorescence polarization, 3TD triple Tudor domain, TD Tudor domain, FL full-length.

occupy both TD aromatic cages simultaneously with another small molecule, MR46747 (PDB: 8UWP), even though their aromatic group binding modes remain different¹⁴.

Design and synthesis of 3TD covalent ligands targeting Cys385

The crystal structure of UNC6535 and the 3TD of SETDB1 revealed that the 6-methoxy group is 5.0 Å from Cys385 while the 7-methoxy moiety is solvent-exposed (Fig. 1b). Therefore, to improve the binding affinity of UNC6535 and its selectivity for the 3TD over the SET domain of SETDB1, a set of nine analogs containing cysteine-targeting electrophilic warheads at position 6 of the quinazoline (1–9) was designed and synthesized (Fig. 1c).

To evaluate the ability of compounds 1–9 to covalently modify SETDB1, the compounds were incubated with SETDB1 3TD protein (10:1 ratio, 2 h incubation at room temperature) and tested by matrix-assisted laser desorption/ionization – time-of-flight (MALDI-TOF) mass spectrometry. Encouragingly, eight out of the nine compounds were able to covalently modify the 3TD of SETDB1, only the methylcarbamate warhead-containing compound (9) did not show any covalent modification of SETDB1 (Supplementary Fig. 4). This might be explained by a longer distance between the electrophilic site of the methylcarbamate and the cysteine as compared to the eight other warheads. Thus, eight covalent analogs of UNC6535 were successfully synthesized and demonstrated the ability to covalently modify SETDB1 3TD by mass spectrometry.

Comparison of eight 3TD covalent hits identified for SETDB1 3TD

Further characterization of the compounds 1–8 was performed to select the most promising hits for further evaluation. A time-dependent MALDI-TOF experiment was conducted to qualitatively evaluate the ability of these compounds to covalently react with the 3TD. After 5 min of incubation with 3TD on ice, all compounds show partial, if not full, covalent bond formation allowing for the qualitative ranking of the compounds for their reactivity towards the 3TD of SETDB1 (Fig. 1d). Warheads such as propiolamide (7) or vinyl sulfonamide (8) showed full covalent modification of the 3TD under these conditions, likely due to their higher intrinsic reactivity. When methylated at the α or β position, acrylamides (1 and 2), and chloroacetamides (3) showed slightly reduced reactivity towards the 3TD compared to the unmethylated (5 and 6) or dimethylamino-modified analogs (4). However, after 30 min of incubation on ice, all of the compounds completely covalently labeled the 3TD demonstrating a high reactivity of all compounds for the 3TD of SETDB1 (Supplementary Fig. 5).

The intrinsic reactivity of the covalent 3TD ligands was evaluated using glutathione (GSH) and was quantified by liquid chromatography–mass spectrometry (LC-MS). Molecules with high intrinsic reactivity are more likely to lack specificity for the target of interest and form covalent bonds with off-target proteins containing reactive cysteines¹⁵. Results showed that the eight covalent SETDB1 ligands had a half-life between 9 min and over 10 days (Table 1 and Supplementary Fig. 6). Compounds with $t_{1/2}$ below 2 h were considered to have risks of off-target reactions and were therefore deprioritized. This led to four promising compounds: UNC10014 (1), UNC10016 (2), UNC9846 (3), and UNC10013 (4).

In parallel, all compounds were tested in a TR-FRET assay to examine their ability to displace the endogenous ligand of the 3TD, H3K9Me2K14Ac (1–25) peptide. Compounds were incubated for 1 h at room temperature before quantification of the FRET signal. All compounds exhibited IC_{50} s between 0.057 and 8.9 μ M, except UNC10015 (5) which increased the TR-FRET signal over the control limit preventing the quantification of the H3K9Me2K14Ac displacement (Table 1 and Supplementary Fig. 7). UNC10013 (4) stood out from the other compounds with a 10-fold potency increase compared to

UNC9970 (7), the second most potent ligand. The different compounds were also tested in the same TR-FRET assay using a cysteine 385 to alanine (C385A) mutant SETDB1 3TD protein. The binding affinities of all covalent compounds decreased compared to the wild-type protein, confirming the role of the covalent bond formation with Cys385 in the binding mode of these compounds (Table 1 and Supplementary Fig. 8).

After confirming that all eight covalent 3TD ligands are efficient at forming a covalent bond with SETDB1, and because the 3TD of SETDB1 contains three different cysteines, Cys314, Cys329, and Cys385, we wanted to evaluate the stoichiometry of the covalent adducts. All the compounds were incubated with the 3TD and submitted for high resolution intact protein mass spectrometry which is more sensitive and accurate than MALDI-TOF for larger proteins such as the 3TD of SETDB1. Results confirmed that compounds 1–8 were fully covalently modifying the 3TD of SETDB1, reinforcing the high reactivity of these small molecules for the 3TD (Supplementary Fig. 9). The main peak for each sample corresponded to the protein modified by one copy of ligand, although compounds UNC9569 (6) and UNC9773 (8) showed minor peaks for the mass corresponding to modification by two ligands. It should be noted that the relative intensity of these peaks was below 6% compared to the intensity of the main peak for the modification of the protein by one copy of ligand and that the protein/ligand concentration ratio was 1:10 which suggests that these 2:1 binding modes could be attributed to the high concentration of ligand (Supplementary Fig. 9). Overall, limited concern about unspecific reactivity for other cysteines of the 3TD was raised.

Compiling all of the data, all compounds were very efficient at forming covalent bonds with the 3TD of SETDB1 and displacing the H3K9Me2K14Ac peptide. However, only four compounds showed GSH $t_{1/2}$ below 2 h, UNC10014 (1), UNC10016 (2), UNC9846 (3) and UNC10013 (4), suggesting reduced potential for off-target covalent bond formation compared to the other four compounds. The substitution of acrylamide or chloroacetamide warheads with methyl or dimethylaminomethyl groups reduced the warhead reactivity but maintained the required geometry necessary for the formation of the covalent bond. Therefore, UNC10014 (1), UNC10016 (2), UNC9846 (3) and UNC10013 (4) were selected for further characterization.

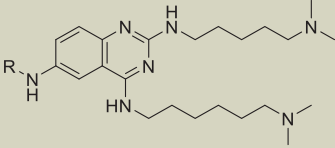
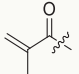
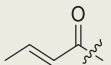
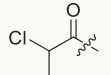
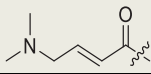
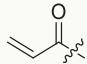
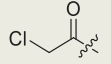
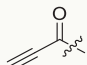
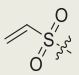
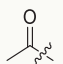
Characterization of four lead covalent ligands for SETDB1 3TD

As mentioned earlier, the 3TD of SETDB1 contains three different cysteines, Cys314, Cys329 and Cys385. We performed LC-MS/MS to identify the cysteines which were covalently modified by the ligands on purified 3TD. Results showed that all four ligands, UNC10014 (1), UNC10016 (2), UNC9846 (3) and UNC10013 (4), modified Cys385 as expected. UNC9846 (3) also showed the ability to covalently modify Cys329 but to a smaller extent than Cys385.

The four best compounds were also evaluated in the SETDB1 methyltransferase activity assay, following three different pre-incubation times of 0, 1, and 2 h. Surprisingly, UNC10014 (1) was the only compound with an IC_{50} dependent on the pre-incubation time (Supplementary Fig. 10). One hypothesis is that UNC10014 (1) is forming a covalent bond with another cysteine among the 36 cysteines of SETDB1 leading to inhibition of the methyltransferase activity. Nevertheless, the three other compounds also exhibited inhibitory properties for the methyltransferase activity of SETDB1 with IC_{50} between 21 and 42 μ M but did not display a dependence on the pre-incubation time, consistent with a reversible mechanism.

To quantitate the targeted covalent reactivity of our best ligands, k_{inact} , the irreversible reaction rate, and K_i , the reversible inhibition constant of the ligand, were assessed for UNC10016 (2), UNC9846 (3), and UNC10013 (4), adapting the previously described TR-FRET system. We examined the time and concentration dependence of our ligands competition with the endogenous ligand, H3K9Me2K14Ac, and

Table 1 | Evaluation of the intrinsic reactivity, binding affinity, and inhibition properties of compounds 1–10 (Supplementary Figs. 6–8)

					
Compound	R =	GSH $t_{1/2}$ (min)	TR-FRET WT IC_{50} (μ M) ^{a,b}	TR-FRET C385A IC_{50} (μ M) ^{a,b}	Methyltransferase IC_{50} (μ M) ^{b,c}
UNC10014 (1)		>10 days	3.1 ± 0.59	12 ± 2.5	54.8 ± 50.5
UNC10016 (2)		>10 days	8.9 ± 3.7	81 ± 11	131 ± 31
UNC9846 (3)		3106	0.80 ± 0.07	9.5 ± 5.4	80.3 ± 52.4
UNC10013 (4)		607	0.057 ± 0.013	8.2 ± 1.8	64.9 ± 47.22
UNC10015 (5)		103	N/A	N/A	0.425 ± 0.135
UNC9569 (6)		60	0.69 ± 0.20	12 ± 4.5 ^d	30.6 ± 32.1
UNC9970 (7)		9	0.66 ± 0.26	31 ± 11.8	6.77 ± 6.03
UNC9773 (8)		23	0.73 ± 0.67	2.5 ± 0.5 ^d	39.9 ± 26.9
UNC9774 (10)		n/a	35 ± 7.1	29 ± 5.1	163 ± 60

Source data are provided as a Source Data file.
 GSH glutathione, TR-FRET time-resolved fluorescence resonance energy transfer, N/A not available.
^aData acquired after 1 h of incubation at rt.
^bValues are reported the average of three biological replicates ± s.d. (n = 3).
^cData acquired after 30 min of incubation at rt.
^dThese compounds showed more than one cysteine simultaneously covalently modified in the 3TD (see Supplementary Fig. 9).

hypothesized that the prevention of binding of the peptide by the tested ligand was a consequence of the formation of the covalent bond with Cys385, as previous mass spectrometry data confirmed that the compounds were efficient at covalently modifying the Cys385 of the 3TD, and the assay was performed with dilution to concentrations below the apparent IC_{50} of the compounds to minimize the reversible binding contribution. For all three compounds, k_{inact} s were comparable ($k_{inact} = 2.61\text{--}6.22 \times 10^{-2} \text{ s}^{-1}$), suggesting similar abilities to form covalent bonds for the three compounds. The differences in K_i were surprising with UNC10013 (4) exhibiting a K_i of $60 \pm 24 \text{ nM}$ while UNC9846 (3) and UNC10016 (2) K_i s were respectively $0.75 \pm 0.35 \mu\text{M}$ and $7.9 \pm 3.4 \mu\text{M}$ (Fig. 2a). This low K_i made UNC10013 (4) a promising lead compound with a k_{inact}/K_i of $1.04 \times 10^6 \text{ M}^{-1} \text{ s}^{-1}$, in the same range as FDA-approved covalent drugs¹⁶.

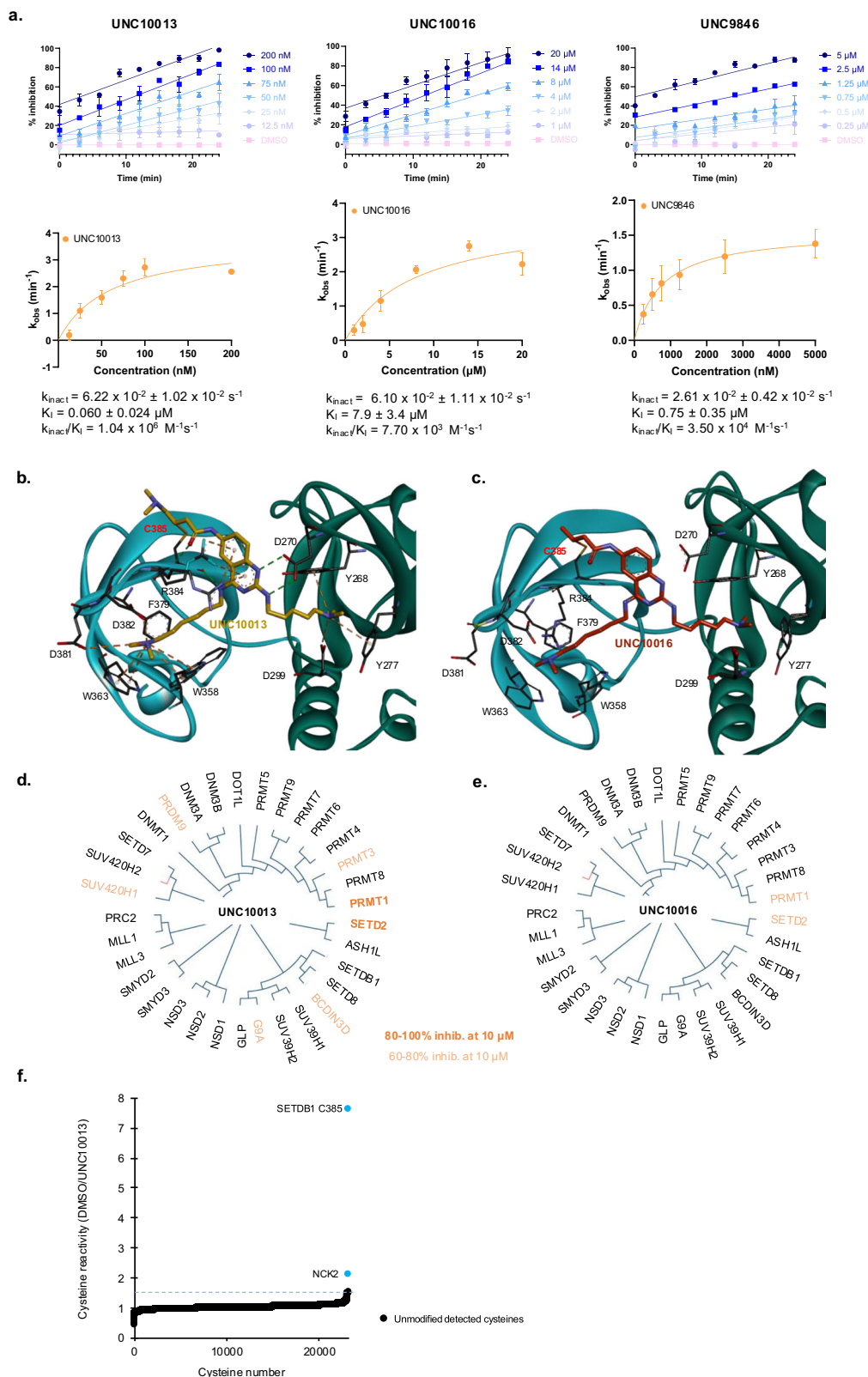
After further characterization of the four lead covalent ligands, UNC10016 (2) and UNC10013 (4) were deemed more attractive for further development as they did not covalently modify other cysteines of SETDB1 thanks to lower intrinsic reactivities, unlike UN9846 (3) and UNC10014 (1), while showing potent k_{inact}/K_i parameters.

Orthogonal binding evaluation of UNC10016 (2) and UNC10013 (4)

Three assays were utilized for the orthogonal binding evaluation of UNC10016 (2) and UNC10013 (4): fluorescence polarization displacement assay, differential scanning fluorimetry (DSF), and a TR-FRET-based nucleosome displacement assay¹⁷. Both UNC10016 (2) and UNC10013 (4) showed potent ability to displace the H3K9Me2K14Ac peptide in the FP assay, with respective IC_{50} s of 0.15 and 0.07 μM at $t = 1 \text{ h}$, validating the compounds as potent 3TD ligands (Table 2 and Supplementary Fig. 11).

DSF evaluation of the ability of ligands to stabilize the 3TD showed significant temperature shifts of 7.0 and 7.7 °C for UNC10013 (4) and UNC10016 (2) respectively (Table 2 and Supplementary Fig. 12). This confirmed the ability of the compounds to bind the 3TD.

Finally, since our prior assays looked at the displacement of H3 tail-mimicking peptides while a natural ligand, the nucleosome, could include different binding components, we examined the 3TD binding to a H3K9Me2K14Ac-modified nucleosome using TR-FRET detection¹⁷. In this assay, we showed that UNC10013 (4) and UNC10016 (2) were able to displace the full nucleosome from the 3TD. UNC10013 (4)



showed a potent IC_{50} of 27 nM, which is similar to the peptide TR-FRET IC_{50} of 57 nM while UNC10016 (2) was less potent with an IC_{50} of 6.3 μM (peptide TR-FRET IC_{50} = 8.9 μM) (Table 2 and Supplementary Fig. 13). These results enhanced our interest in further developing UNC10013 (4) and UNC10016 (2) into covalent chemical tools to study the interaction of the 3TD with the nucleosome and other substrates.

Covalent chemical probe criteria evaluation for UNC10016 (2) and UNC10013 (4) candidates

Chemical probe experts have agreed on the criterion required for a covalent chemical probe¹⁸:

1. Biophysical proof of target engagement
2. Known k_{inact}/K_i

Fig. 2 | Covalent chemical probe criteria evaluation for UNC10016 (2), UNC9846 (3) and UNC10013 (4). **a** Kinetic parameters k_{inact}/K_i evaluation for UNC10016 (2), UNC9846 (3), and UNC10013 (4) using a TR-FRET displacement assay. The inhibition at different time points for different concentrations of compound were measured and plotted as a function of time. Resulting slopes, corresponding to k_{obs} were plotted as a function of the concentration to calculate k_{inact} and K_i values. Reported values are the average of three biological replicates \pm s.d. ($n = 3$). **b** Crystal structure of UNC10013 (4) (left) and **c** UNC10016 (2) (right) bound to SETDB1 3TD (PDB ID: 9CUX, 9CUW) Visualized with Discovery Studio. Cation- π interactions are shown in orange. H-bond interactions are shown in green. **d** Phylogenetic tree of

the 33 methyltransferases tested for off-target activity of UNC10013 (4) and **e** UNC10016 (2) using a radiometric methyltransferase assay. Values are the average of three biological replicates ($n = 3$). Proteins in light orange showed 60–80% inhibition by tested compounds at 10 μM . Proteins in dark orange showed over 80% inhibition by tested compounds at 10 μM (see Supplementary Table S1). **f** Plot showing the relative cysteine reactivity of 23,149 detected cysteines after treatment of MCF-7 cell lysate with 10 μM of UNC10013 (4) compared to DMSO. Two cysteines showed significant cysteine reactivity, SETDB1 Cys385 and NCK2 Cys144 (>1.5). Source data are provided as a Source Data file.

Table 2 | Binding, selectivity, and permeability evaluation of UNC10013 (4) and UNC10016 (2) (see Supplementary Figs. 11–13)

Assay		UNC10013 (4)	UNC10016 (2)
FP IC ₅₀ (μM) ^a		0.07 \pm 0.01	0.15 \pm 0.04
DSF ΔT_m ($^{\circ}\text{C}$) ^b		7.0 \pm 0.1	7.7 \pm 0.2
Nucleosome TR-FRET IC ₅₀ (μM) ^a		0.027 \pm 0.005	6.3 \pm 1.4
Selectivity Evaluation	SETDB1 3TD	0.057 \pm 0.013	8.9 \pm 3.7
	53BP1 TTD	20 \pm 5.6 (>100 -fold)	>100
	CHD1 CD	43 \pm 4.2 (>100 -fold)	11 \pm 3.1
	MPP8 CD	90 \pm 15 (>100 -fold)	16 \pm 3.8
TR-FRET IC ₅₀ (μM) ^a	CBX2 CD	>100	>100
	CDYL2 CD	>100	>100
	PHF1 TD-PHD-PHD	>100	>100
	PHF19 TD-PHD	>100	>100
	KDM7B JmjC-PHD	>100	>100
Assay		UNC10013 (4)	(R,R)–59
CeTSA ΔT_m ($^{\circ}\text{C}$) ^a	HiBIT-3TD	0.89	0.95
	HiBIT-3TD + Digitonin	6.29	0.39

Source data are provided as a Source Data file.

FP fluorescence polarization, DSF differential scanning fluorimetry, TR-FRET time-resolved fluorescence resonance energy transfer, CeTSA cellular thermal shift assay, 3TD triple Tudor domain, TTD tandem Tudor domain, CD chromodomain, PHD plant homeodomain, JmjC Jumonji C.

^aValues are reported as the average of three biological replicates \pm s.d. ($n = 3$).

^bValues are reported as the average of two biological replicates \pm s.d. ($n = 2$).

3. Target family selectivity (> 30 -fold)
4. Proteome-wide selectivity
5. Availability of inactive control
6. Cellular potency ($< 1 \mu\text{M}$)

Promising results from the characterization of UNC10016 (2) and UNC10013 (4) led to the evaluation of both ligands as chemical probe candidates applying each of the six criteria. One of the criteria, knowing the k_{inact}/K_i , being already addressed in our initial studies.

Co-crystallization of UNC10016 (2) and UNC10013 (4) in the 3TD.

Co-crystallization of UNC10016 (2) and UNC10013 (4) within the 3TD confirmed that both compounds maintained binding poses similar to UNC6535 while covalently engaging Cys385 (Fig. 2b, c). Additional interactions between the backbone of Cys385 and the carbonyl of UNC10013 (4) and UNC10016 (2) were observed while only the UNC10013 (4) quinazoline core showed some cation- π interactions with Arg384 which might explain its improved K_i . Overall, the X-ray crystallography data met criterion 1 for a covalent chemical probe while highlighting the ability of these compounds to

occupy the aromatic cages of both TD2 and TD3 of the 3TD of SETDB1 simultaneously while covalently modifying Cys385.

Selectivity evaluation: family and proteome-wide. A screen of UNC10016 (2) and UNC10013 (4) against various Kme reader proteins using similar TR-FRET technology as for SETDB1 was initiated¹⁹. Results showed that UNC10013 (4) was at least 100-fold selective against the eight Kme readers tested, which included various Kme sub-families such as Tudor domains, chromodomains, and PHD domains (Table 2). Unfortunately, UNC10016 (2) lacked selectivity against the chromodomains of CHD1 and MPP8.

SETDB1 also contains a lysine methyltransferase domain which modifies substrates similar to the 3TD ligands, so we expanded the family selectivity evaluation to the methyltransferase family. The ability of thirty-three methyltransferases to modify lysine and arginine-containing substrates was tested in the presence of a single concentration of 10 μM of UNC10013 (4) and UNC10016 (2). UNC10013 (4). Confirming our previous results, no inhibition of the SETDB1 methyltransferase activity was observed at 10 μM . This assay also showed at least 60% inhibition for seven methyltransferases, two of them, SETD2 and PRMT1, showed over 80% inhibition at 10 μM (Fig. 2d, e and Supplementary Table 1). Accordingly, a full dose-response evaluation of the ability of UNC10013 (4) to inhibit SETD2 and PRMT1 methyltransferase activities was performed. UNC10013 (4) is selective for the binding of the 3TD of SETDB1 by 30-fold relative to SETD2 inhibition ($\text{IC}_{50} = 0.8 \pm 0.1 \mu\text{M}$), and 48-fold relative to PRMT1 inhibition ($\text{IC}_{50} = 1.3 \pm 0.1 \mu\text{M}$) (Supplementary Fig. 14). Although this data suggests that UNC10013 (4) marginally meets the covalent chemical probe criterion for selectivity (>30 -fold), it should be noted that UNC10013 (4) is covalently modifying the 3TD of SETDB1 while no proof of covalent modification of the methyltransferases SETD2 and PRMT1 was observed in the ABPP (Fig. 2f).

Regarding UNC10016 (2), while fewer methyltransferases were inhibited with the compound at 10 μM , both SETD2 and PRMT1 showed over 60% inhibition suggesting similar binding affinities compared to the 3TD (3TD $\text{IC}_{50} = 6.3 \pm 1.4 \mu\text{M}$). Based on the lack of selectivity for both the Kme reader and methyltransferase proteins, UNC10016 was deprioritized for development as a covalent chemical probe.

Cysteine-targeted activity-based protein profiling (ABPP) was used to evaluate the proteome-wide selectivity of UNC10013 (4). Results showed that out of 23,149 detected cysteines in the native MCF-7 proteome, remarkably UNC10013 (4) preferentially modified SETDB1 at Cys385 relative to 22 other cysteines also present in SETDB1 (Fig. 2f and Supplementary Table 2), and only one off-target NCK2 (Cys144) was detected.

Overall, characterization of the selectivity of UNC10013 (4) and UNC10016 (2) demonstrated that UNC10013 (4) has a promising selectivity profile as a covalent chemical probe candidate. We identified two methyltransferase proteins as potential off-targets, which suggests that cellular applications should proceed with consideration of methyltransferase inhibition as a possible confounding activity.

Inactive control development. To facilitate cellular studies, a negative control analog that retains the covalent warhead of UNC10013 (4) was developed. One strategy was to replace the TD2-occupying basic

center with neutral heteroatom-containing groups to prevent the key cation- π interaction with the TD2 aromatic cage. Therefore, the dimethylamine group was replaced by a methoxy (UNC1277 (**11**)) or an

acetamide group (UNC1366 (**12**)) by adapting the synthetic route of UNC10013 (**4**) (Fig. 3a).

The two negative controls were evaluated using MALDI-TOF for their ability to form a covalent bond with SETDB1 3TD. Results showed that both compounds **11** and **12** retained the ability to form a covalent bond with the 3TD but at a slower rate than UNC10013 (**4**). This confirmed a decrease in affinity after removal of the basic center in the TD2. After 5 min of incubation on ice, most 3TD remained unmodified by UNC1277 (**11**) and UNC1366 (**12**) while UNC10013 (**4**) completely covalently modified the protein (Fig. 3b). While compounds **1–8** showed complete covalent labeling after 30 min (Supplementary Fig. 5), UNC1277 (**11**) and UNC1366 (**12**) showed partial covalent labelling suggesting a lower reactivity towards covalent modification of SETDB1 (Fig. 3b). After 2 h of incubation on ice, both negative control candidates **11** and **12** showed a nearly complete covalent modification of SETDB1, confirming their ability to covalently modify the 3TD of SETDB1 (Supplementary Fig. 15).

In order to quantify their reactivity for SETDB1, both compounds **11** and **12** were tested in the TR-FRET and FP displacement assays. UNC1277 (**11**) (IC_{50} = 20 μ M), and UNC1366 (**12**) (IC_{50} = 9.0 μ M) showed over 100-fold selectivity in the TR-FRET assay compared to UNC10013 (**4**) (IC_{50} = 0.057 μ M) (Fig. 3a and Supplementary Fig. 16). However, in the FP assay, UNC1277 (**11**) and UNC1366 (**12**) showed a 10-fold (IC_{50} = 0.80 μ M) and a 7-fold selectivity (IC_{50} = 0.56 μ M) respectively (Fig. 3a and Supplementary Fig. 17). These results suggest that UNC1277 (**11**) and UNC1366 (**12**) are promising negative controls with lower reactivity towards the covalent modification of the 3TD of SETDB1 than UNC10013 (**4**) and decreased binding ability.

Cellular target engagement evaluation. One key characteristic of chemical probes is their ability to potently engage the target of interest in cells. First, a cell viability evaluation was performed to ensure UNC10013 (**4**) and its negative control, UNC1277 (**11**), were not toxic to the cells. Treatment of MCF-7 cells with concentrations up to 50 μ M for 24 h, 48 h, and 72 h did not result in a cell viability decrease compared to DMSO (Supplementary Fig. 18).

Another key parameter to ensure that small molecules can engage the target of interest in cells is cell permeability. To evaluate the cell permeability of UNC10013 (**4**), a Caco-2 evaluation was performed. Although no concerning efflux ratio was measured (Efflux ratio = 1.11), a low apparent permeability P_{app} (A-B) was observed (P_{app} (A-B) = 0.37×10^{-6} cm/s; P_{app} (B-A) = 0.41×10^{-6} cm/s) suggesting modest cell permeability. This result is likely associated with the fact that UNC10013 (**4**) contains three basic amines and three H-bond donor groups.

The cellular thermal shift assay (CeTSA) was used to evaluate target engagement of UNC10013 (**4**). HEK293T cells were transfected with SETDB1 3TD tagged with HiBIT and incubated with 30 μ M of UNC10013 (**4**) or (*R,R*)-59, a known 3TD cellular ligand, used as a positive control. Similar ΔT_m were measured for both UNC10013 (**4**) and the positive control (*R,R*)-59, 0.89, and 0.95 $^{\circ}$ C respectively, although the thermal shifts remained small (Table 2). Concerns about the low cell permeability of UNC10013 (**4**) led us to reproduce the CeTSA results using cells permeabilized by digitonin. Indeed, a ΔT_m of 6.29 $^{\circ}$ C was measured under this condition, similar to the in vitro ΔT_m for UNC10013 (**4**) and the 3TD (Table 2). The significant increase of ΔT_m upon permeabilization of the cells confirms that UNC10013 (**4**) has low cell permeability decreasing its potency in cellular assays. Surprisingly, (*R,R*)-59 treatment of digitonin-permeabilized cells showed a decrease in ΔT_m compared to unpermeabilized cells potentially possibly due to cellular toxicity. Overall, we confirmed that UNC10013 (**4**) is able to engage the 3TD in cells at 30 μ M although this ability is impaired due to low cell permeability.

Covalent chemical probe summary. To sum up, UNC10013 (**4**) has shown potent k_{inact}/K_i kinetic parameters for covalently binding the

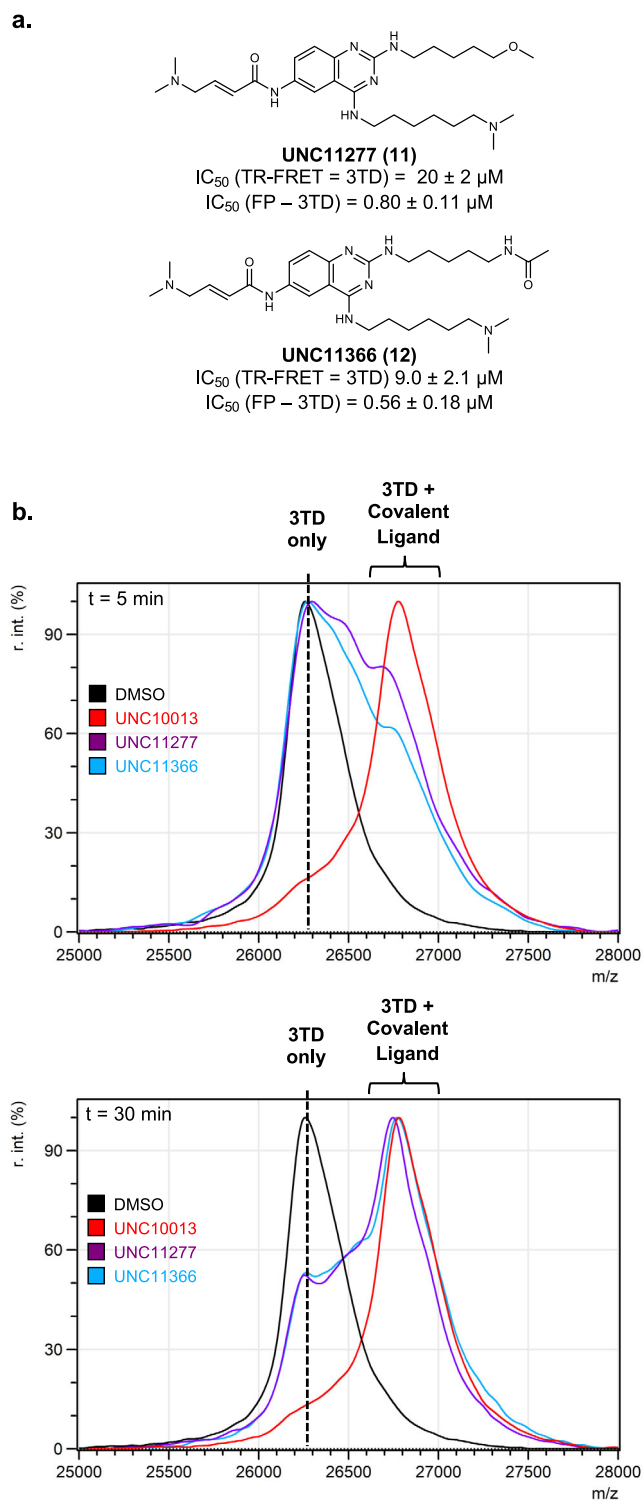


Fig. 3 | Characterization of negative control candidates UNC1277 (11**) and UNC1366 (**12**).** **a** Structure and binding evaluation of UNC1277 (**11**) and UNC1366 (**12**). Reported values are the average of three biological replicates \pm s.d. (n = 3). Source data are provided as a Source Data file. **b** Representative MALDI-TOF qualitative evaluation of the ability of UNC10013 (**4**) (red) UNC1277 (**11**) (purple), and UNC1366 (**12**) (blue) to covalently modify SETDB1 3TD after t = 5 min (top) and t = 30 min (bottom) incubation on ice. TR-FRET time-resolved fluorescence resonance energy transfer, FP fluorescence polarization, 3TD triple Tudor domain.

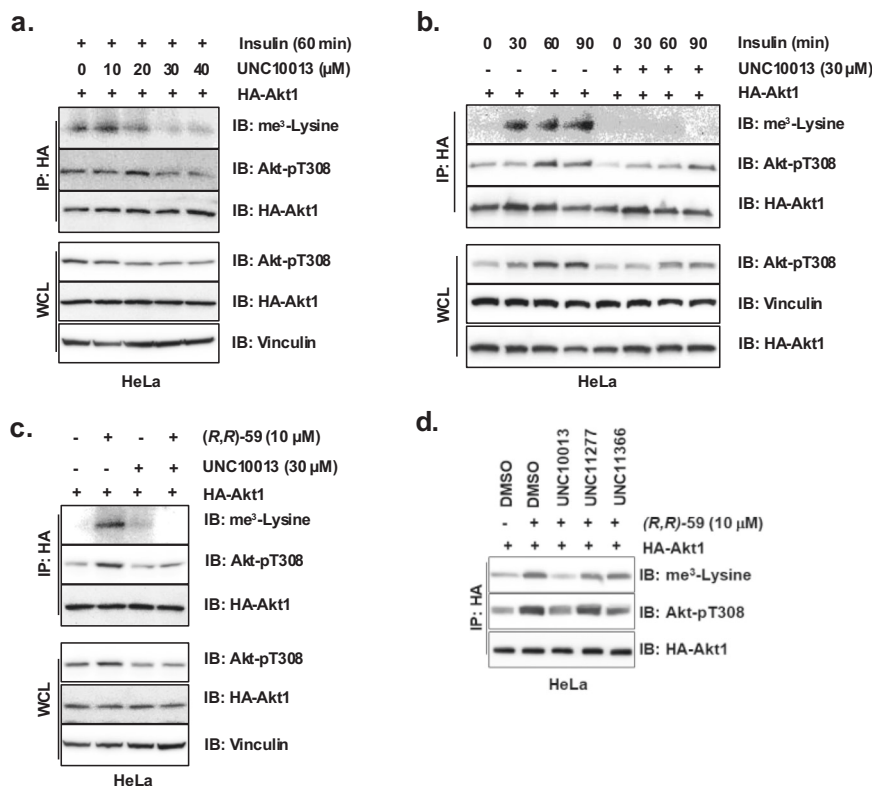


Fig. 4 | Cellular evaluation of UNC10013 (4) and UNC11277 (11) for the modulation of the SETDB1-mediated Akt methylation activity reveals negative allosteric modulation properties of UNC10013. **a** Pretreatment with different concentration of UNC10013 (4) for 24 h followed by 60 min of insulin stimulation of the Akt methylation. **b** Pretreatment with 30 μ M of UNC10013 (4) for 24 h followed by different insulin stimulation treatment times. **c** Cotreatment with

10 μ M of (*R,R*)-59 and 30 μ M of UNC10013 (4) for 24 h. **d** Pretreatment with 30 μ M of UNC10013 (4), UNC11277 (11) or UNC11366 (12) for 2 h followed by treatment with 10 μ M of UNC8830 for 18 h. Two biological replicates with similar results were obtained for each experiment ($n = 2$). Source data are provided as a Source Data file. IB immunoblot, IP immunoprecipitation, WCL whole cell lysate, HA hemagglutinin.

3TD of SETDB1. We confirmed that the modified cysteine is Cys385 by LC-MS/MS and X-ray crystallography. Proteome-wide selectivity evaluation of UNC10013 (4) showed only Cys144 of NCK2, an adaptor protein unrelated to SETDB1, covalently modified by UNC10013 (4) along SETDB1 Cys835, resulting in an off-target rate of 0.004% out of 23,149 detected cysteines. We achieved target family selectivity against a panel of methyltransferases and Kme readers in biophysical assays as well. Then, we identified UNC11277 (11) as a structurally related negative control, which contains the same covalent warhead as UNC10013 (4), for cellular assays. Finally, UNC10013 (4) did not show toxicity for cellular treatment of MCF-7 for concentrations up to 50 μ M and showed cellular target engagement of SETDB1 3TD at 30 μ M in CeTSA. Unfortunately, UNC10013 (4) has low cell permeability, as shown in Caco-2 evaluation and in CeTSA, which reduces its ability to potentially engage its target in cells.

Five out of the six criteria for a covalent chemical probe were validated for UNC10013 (4) demonstrating that UNC10013 (4) is an excellent starting point for the development of a SETDB1 3TD covalent chemical probe. Nevertheless, although we did not engage SETDB1 in cells at concentrations below 1 μ M, UNC10013 (4) remains an exciting chemical tool to study the 3TD of SETDB1. Indeed, we observed binding to the 3TD at 30 μ M by CeTSA, suggesting that higher concentrations of compound will likely be required to compensate for the low cell permeability.

UNC10013 is a negative allosteric modulator of the methyltransferase activity of SETDB1

Next, we examined whether UNC10013 (4) would influence the allosteric relationship between the 3TD and the methyltransferase domains

that we previously observed¹³. While H3K9 methylation is not SETDB1-specific, the only known Akt methylation effector is SETDB1^{9,10}. Accordingly, we looked at the ability of UNC10013 (4) to modulate the SETDB1-mediated Akt methylation in HeLa cells after insulin stimulation. First, cells were pretreated for 24 h with different concentrations of UNC10013 (4) before the Akt methylation was triggered for 60 min using insulin (Fig. 4a). Results showed that treatment with 30 μ M or more of UNC10013 (4) inhibited Akt methylation and subsequent Akt Tyr308 phosphorylation. Further evaluation of UNC10013 (4) showed that the compound was able to inhibit Akt methylation and subsequent phosphorylation after insulin activation up to 90 min, suggesting a robust inhibition (Fig. 4b).

Previous studies showed that the small-molecule 3TD ligand for SETDB1, (*R,R*)-59, is a positive allosteric modulator of the methyltransferase activity of SETDB1¹³. Therefore, we decided to use (*R,R*)-59, instead of insulin, to activate the SETDB1-mediated Akt methylation. In this system, we observed that co-treatment with 10 μ M of (*R,R*)-59 and 30 μ M of UNC10013 (4) inhibited the (*R,R*)-59-triggered Akt methylation and phosphorylation (Fig. 4c). In another experiment, we found that pretreatment with 30 μ M of UNC10013 (4), but not the negative control UNC11277 (11), for 2 h was able to prevent (*R,R*)-59-induced Akt methylation treatment in HeLa cells (Fig. 4d). The lack of efficacy of UNC11277 (11) is a consequence of its much diminished k_{inact}/K_i and the low permeability of this series²⁰.

Knowing that (*R,R*)-59 and UNC10013 (4) share the same binding pocket, these results demonstrate that UNC10013 (4) is a negative allosteric modulator of the methyltransferase domain of SETDB1, competing with (*R,R*)-59, and confirm that the 3TD is an allosteric site able to modulate the catalytic activity of the methyltransferase domain

of SETDB1. This is significant because inhibitors of the catalytic SET domain have not yet been advanced as potential anti-cancer drugs and targeting the 3TD with negative allosteric modulators may provide this therapeutic opportunity. These experiments also suggest that UNC1277 (**11**) is a good negative control for UNC10013 (**4**) in cells.

Discussion

In these studies, we identified UNC6535 as a small molecule ligand for the SETDB1 3TD able to occupy both the TD2 and TD3 aromatic cages simultaneously. UNC6535 showed a K_d of 4.2 μ M for the 3TD and the ability to displace the H3K9Me2K14Ac peptide-mimicking the endogenous histone tail. Subsequent structure-based design identified UNC10013 (**4**) as a promising covalent chemical tool for the 3TD of SETDB1. X-ray crystallography confirmed that UNC10013 (**4**) maintains the binding pose of UNC6535 while covalently modifying Cys385. UNC10013 (**4**) has a potent k_{inact}/K_i of $1.04 \times 10^6 \text{ M}^{-1} \text{ s}^{-1}$ and excellent proteome-wide selectivity. We also demonstrated that it could potentially displace the H3K9Me2K14Ac-modified entire nucleosome from the 3TD. Caco-2 cell permeability, and CeTSA cellular target engagement evaluations revealed low cell permeability. However, UNC10013 (**4**) was able to engage the 3TD in HEK293T cells at 30 μ M. Indeed, using SETDB1-mediated Akt methylation as a functional readout, we observed that UNC10013 (**4**) is a negative allosteric modulator of the methyltransferase activity of SETDB1 at concentrations of 30 μ M and above revealing the ability to inhibit the methyltransferase activity of SETDB1 by targeting its 3TD.

In conclusion, we identified UNC10013 (**4**), a covalent ligand for the 3TD of SETDB1, and demonstrated that it can allosterically inhibit the methyltransferase activity of SETDB1 in cells. This chemical tool complements the previously identified (*R,R*)-59 compound which is a positive allosteric modulator of SETDB1 catalytic activity and also binds the 3TD. Indeed, this pair of compounds should allow researchers to gain a better understanding of the function of the 3TD of SETDB1 and its relationship with the other domains, especially the methyltransferase domain.

Allosteric modulators are especially attractive since the SET domain of methyltransferases is highly conserved within the family, therefore drugging the allosteric Kme reader domain is a promising strategy to potentially achieve selectivity for SETDB1 SET domain inhibition. Moreover, decrease in Akt methylation and subsequent phosphorylation achieved by SETDB1 depletion has been linked to decreased tumor growth in vivo¹⁰. Therefore, the development of an allosteric negative modulator ligand for the 3TD of SETDB1 is a promising approach to develop cancer or neurological disorder-targeting therapies, especially as there are currently no structural data or potent confirmed molecules directly targeting the methyltransferase SET domain^{21,22}.

In the future, we intend to address the cell permeability issues of UNC10013 (**4**) by structural modifications and cellular evaluation to provide a more potent 3TD covalent chemical probe for cellular studies.

Methods

Protein and peptide production and purification

Expression constructs. The chromo domains of CBX2 (residues 9–66 of NP_005180) and MPP8 (residues 55–116 of NP_059990) were expressed with N-terminal His-tags in modified pET28 expression vectors. The chromo domain of CDYL2 (residues 1–75 of NP_689555) was expressed with a C-terminal His-tag in a pET30 expression vector. The Tudor domain of SETDB1 (residues 196–403 of NP_036564) was expressed with an N-terminal His-tag in a modified pET28 expression vector. The SETDB1 C385A mutant was generated using a QuickChange II site-directed mutagenesis kit (Agilent) according to manufacturer's recommendations. The Tudor domain of 53BP1 (residues 1484–1603 of NP_005648) was expressed with an N-terminal His tag in a pET15

expression vector. The Tudor and PHD domains of PHF1 (residues 27–360 of NP_077084) and PHF19 (residues 1–207 of NP_001009936) were expressed with N-terminal His-tags in modified pET28 expression vectors. The Jumonji domain of KDM7B (residues 1–447 of NP_055922) was expressed with an N-terminal MBP-tag and a C-terminal His-tag. Full length SETDB1 (residues 1–1291 of NP_001138887) was expressed in a pFastBac baculovirus expression vector with an N-terminal His-tag and a C-terminal FLAG tag. Truncated SETDB1 (residues 570–1291 of NP_001138887) was expressed with a N-terminal GST and His-tag in a pFastBac baculovirus expression vector.

Protein expression and purification. All *E. coli* expression constructs were transformed into Rosetta BL21(DE3)pLysS competent cells (Novagen, MilliporeSigma). Protein expression was induced by growing cells at 37 °C with shaking until the OD600 reached 0.6–0.8 at which time the temperature was lowered to 18 °C and expression was induced by adding 0.5 mM IPTG and continuing shaking overnight. Cells were harvested by centrifugation and pellets were stored at –80 °C.

All His-tagged proteins except for KDM7B were purified by resuspending thawed cell pellets in 30 ml of lysis buffer (50 mM sodium phosphate pH 7.2, 50 mM NaCl, 30 mM imidazole, 1X EDTA free protease inhibitor cocktail (Roche Diagnostics) per liter of culture. Cells were lysed on ice by sonication with a Branson Digital 450 Sonifier (Branson Ultrasonics) at 40% amplitude for 12 cycles with each cycle consisting of a 20 s pulse followed by a 40 s rest. The cell lysate was clarified by centrifugation and loaded onto a HisTrap FF column (Cytiva) that had been preequilibrated with 10 column volumes of binding buffer (50 mM sodium phosphate pH 7.2, 500 mM NaCl, 30 mM imidazole) using an AKTA FPLC (Cytiva). The column was washed with 15 column volumes of binding buffer and protein was eluted in a linear gradient to 100% elution buffer (50 mM sodium phosphate pH 7.2, 500 mM NaCl, 500 mM imidazole) over 20 column volumes. Peak fractions containing the desired protein were pooled and concentrated to 2 ml in Amicon Ultra-15 concentrators 3,000 molecular weight cut-off (Merck Millipore). Concentrated protein was loaded onto a HiLoad 26/60 Superdex 75 prep grade column (Cytiva) that had been preequilibrated with 1.2 column volumes of sizing buffer (25 mM Tris pH 7.5, 250 mM NaCl, 0.5 mM TCEP, 5% glycerol for MPP8 or 25 mM Tris pH 7.5, 250 mM NaCl, 2 mM DTT, 5% glycerol for all other proteins) using an ATKA Purifier (Cytiva). Protein was eluted isocratically in sizing buffer over 1.3 column volumes at a flow rate of 2 ml/min collecting 3 ml fractions. Peak fractions were analyzed for purity by SDS-PAGE and those containing pure protein were pooled and concentrated using Amicon Ultra-15 concentrators 3000 molecular weight cut-off (Merck Millipore).

KDM7B purification. KDM7B was purified as described above for His-tagged proteins with the following exceptions. Peak fractions from the HisTrap column were pooled and concentrated in Amicon Ultra-15 concentrators 50,000 molecular weight cut-off (Merck Millipore). The N-terminal MBP tag was removed by TEV cleavage as described above for MPP8. The cleavage reaction was then passed over a HisTrap FF column (Cytiva) to remove any protein that still retained the tag as well as the His-tagged TEV protease. The column flow through was collected and concentrated to 2 ml using Amicon Ultra-15 concentrators, 30,000 molecular weight cut-off (Merck Millipore). Concentrated protein was loaded onto a HiLoad 26/60 Superdex 200 prep grade column (Cytiva) that had been preequilibrated with 1.2 column volumes of sizing buffer (25 mM Tris pH 7.5, 250 mM NaCl, 2 mM DTT, 5% glycerol) using an ATKA FPLC (Cytiva). Protein was eluted isocratically in sizing buffer over 1.3 column volumes at a flow rate of 2 ml/min collecting 3 ml fractions. Peak fractions were analyzed for purity by SDS-PAGE and those containing pure protein were pooled and concentrated using Amicon Ultra-15 concentrators 30,000 molecular weight cut-off (Merck Millipore).

Baculovirus expression and purification. Baculoviruses for full length and truncated SETDB1 were generated using the Bac-to-Bac expression system (Invitrogen). Sf9 cells were grown in Sf900III SFM media (Gibco) supplemented with 2%FBS to 1×10^6 cells/ml and infected at an MOI of 5 with a baculovirus containing either full length SETDB1 or truncated SETDB1. Cells were harvested after 72 h, and cell pellets were stored at -80°C until purification.

Truncated SETDB1 purification. Cell pellets from 1 L of infected cells were thawed and resuspended in 30 ml of cytobuster (Merck Millipore) containing 1X EDTA free protease inhibitor cocktail (Pierce), 1X phosphatase inhibitor cocktail (Pierce) and 30 mM imidazole, pH 8.0. Cells were lysed for 15 min at room temperature with gentle mixing. Cell lysates were clarified by centrifugation and the clarified supernatant was loaded onto a 1 ml HisTrapFF column (Cytiva) that had been preequilibrated with 10 column volumes of binding/wash buffer (50 mM sodium phosphate, pH 7.2, 500 mM NaCl, 30 mM imidazole) at a flow rate of 1 ml/min using an AKTA FPLC (Cytiva). The column was washed with 15 column volumes of binding/wash buffer and bound protein was eluted in a linear gradient over 20 column volumes to 100% elution buffer (50 mM sodium phosphate buffer, pH 7.2, 500 mM NaCl, 500 mM imidazole). Peak fractions were run on SDS-PAGE gels and analyzed by Coomassie staining. Truncated SETDB1 containing fractions were pooled and concentrated in Amicon Ultra 30 K cut off concentrators (Merck Millipore) and buffer was exchanged into 25 mM HEPES, pH 7.5, 300 mM NaCl, 0.5 mM TCEP, 10% glycerol, 0.04% Triton. Protein concentration was determined by Bradford assay. Protein was aliquoted and stored at -80°C .

Full-length SETDB1 purification. Cell pellets from 1 L of infected cells were thawed and resuspended in 30 ml of cytobuster (Merck Millipore) containing 1X EDTA free protease inhibitor cocktail (Pierce), and 1X phosphatase inhibitor cocktail (Pierce). Cells were lysed for 15 min at room temperature with gentle mixing. Cell lysates were clarified by centrifugation and the clarified supernatant was incubated with ANTI-FLAG M2 affinity gel (Sigma) overnight at 4° . The FLAG gel was washed with TBS and protein was eluted by competition with FLAG peptide (Sigma). Elution fractions were run on SDS-PAGE gels and analyzed by Coomassie staining. Full length SETDB1 containing fractions were pooled and concentrated in Amicon Ultra 50 K cut off concentrators (Merck Millipore) and buffer was exchanged into 25 mM HEPES, pH 7.5, 300 mM NaCl, 0.5 mM TCEP, 10% glycerol, 0.04% Triton. Protein concentration was determined by Bradford assay. Protein was aliquoted and stored at -80°C .

Peptide production. H3K9Me2K14Ac-Biotin (aa 1–19) peptide was purchased from Genscript. The countersalts are hydrochloric salts. The sequence is as followed:

H3K9Me2K14Ac-Biotin (aa 1–19): MARTKQTAR{Lys(me3)}STGG{Lys-Ac}APRKQ{K(Biotin)}.

Nucleosome production and purification

Preparation of histone peptide and protein fragments for expressed protein ligation. Peptide 1, containing H3.2(1–23, K9Me2, K14Ac, C-terminal hydrazide) was synthesized by the UNC High-throughput Peptide Synthesis and Array Facility, purified by reverse phase HPLC (RP-HPLC), and confirmed by MALDI spectrometry. The gene sequence encoding human H3.2 residue 24–135 was cloned into the pST50Tr vector with an N-terminal TEV protease cleavage sequence (ENLYFQ) and A24C and C110A mutations. ENLYFQ-H3.2 (24–135, A24C, C110A, hereafter, H3.2-C) was expressed in *E. coli* BL21(DE3) pLys cells at 37°C for 3 h. The ENLYFQ-H3.2-C protein was extracted from inclusion bodies as previously described²³ and dialyzed overnight into 0.1% TFA in water at 4°C . The dialyzed protein was cleared by centrifugation and filtration (0.45 μm) and purified by RP-HPLC (Vydac

218TP C18 column, 250×22 mm, 10 μm) using a 40–70% B gradient over 60 min (A: 0.1% TFA in water; B: 90% acetonitrile, 0.1% TFA in water) and lyophilized. The identity of the ENLYFQ-H3.2-C protein was verified by LC/MS. The purified H3.2-C protein was dissolved in 50 mM Tris-HCl, pH 8.0, 1 mM DTT, 0.5 mM EDTA, 6 M guanidine HCl (GnCl) and then diluted in the same buffer lacking GnCl to a final concentration of 1 M GnCl and 1 mg/ml protein. The ENLYFQ sequence was cleaved with the addition of 1/100 molar eq TEV protease for 2 h at room temperature and purified by RP-HPLC exactly as described above, yielding H3.2-C protein 2.

Expressed protein ligation. The expressed protein ligation reaction between peptide 1 and H3.2-C protein 2 was performed essentially as previously described (Fig. 5)²⁴. Briefly, peptide 1 (0.9 mg, 0.35 μmol) was dissolved in 70 μl of 0.2 M phosphate containing 6 M GnCl (pH 3.0–3.1). The peptide hydrazide was converted to an azide by addition of 10 molar equivalents of NaNO_2 using a 0.5 M NaNO_2 stock. This reaction was allowed to proceed for 15–20 min at -15°C in an ice/salt bath. The H3.2-C protein 2 (4.1 mg, 0.32 μmol) was dissolved in 70 μl of 0.2 M phosphate containing 6 M GnCl (pH 6.8–7.0) containing 100 molar eq of 4-mercaptophenylacetic acid (MPAA, Sigma) and added to the peptide. The pH of the ligation mixture was adjusted to 6.8–7.0 and the ligation was allowed to proceed for 24 h at room temperature, affording H3.2K9me2K14ac(A24C, C110A), 3. Ligation product 3 was purified by RP-HPLC (Vydac 218TP C18 column, 250×10 mm, 5 μm) with a 43–53% B gradient over 45 min, yielding 2.3 mg. The identity of the ligation product was verified by LC/MS.

Preparation of nucleosomes. The human H3.2(A24C, C110A) mutant was cloned in the pST50Tr vector by site-directed mutagenesis. Human histones H2A, H2B, H3.2(A24C, C110A), and H4 were expressed and purified from inclusion bodies as previously described²³. H2A(K119C)/H2B dimer, H3.2K9me2K14ac(A24C, C110A)/H4 tetramer, and unmodified, control H3.2(A24C, C110A)/H4 tetramer were reconstituted and purified by cation exchange chromatography as previously described²⁵. The H2A(K119C)/H2B dimer was labeled with biotin-maleimide exactly as previously described¹⁷. Modified H2A(K119C-biotin)/H2B/H3.2K9me2K14ac(A24C, C110A)/H4 and unmodified H2A(K119C-biotin)/H2B/H3.2(A24C, C110A)/H4 nucleosomes were assembled with 185 bp 601 nucleosome positioning sequence²⁶ with 20 bp symmetric linker DNA and purified as previously described^{23,25}.

TR-FRET displacement assay

H3K9Me2K14Ac peptide displacement from SETDB1 3TD. The TR-FRET assay protocol was developed and adapted from a previously reported protocol¹⁹. Briefly, the assay was run using white, low-volume, flat-bottom, nonbinding, 384-well microplates (Greiner, 784904) containing a total volume of 10 μl per well. The buffer was made of 1X PBS pH 7.0, 0.005% Tween 20, and 2 mM DTT. Lance Europium (Eu)-W1024 Streptavidin conjugate (2 nM) and LANCE Ultra ULIGHTM-anti-6x-His antibody (10 nM) were used as donor and acceptor fluorophores associated with the tracer ligand and protein respectively. Final assay concentrations of 40 nM 6X histidine-tagged SETDB1 (residues 195–403, N-terminal tag) and 40 nM of H3K9Me2K14Ac-Biotin (aa 1–19) were used for compound testing. A 10-point, three-fold serial dilution of each compound was tested as the primary hit validation. Assay components were added to an assay plate using a Multidrop Combi (ThermoFisher). After addition, the plates were sealed with clear covers, mixed gently on a shaker for 1 min, centrifuged at $1000 \times g$ for 2 min, and allowed to equilibrate for 1 h in the dark. Plates were read with an EnVision 2103 Multilabel Plate Reader (PerkinElmer) using an excitation filter at 320 nm and emission filters at 615 and 655 nm. Emission signals (615 and 655 nm) were measured simultaneously using a dual mirror D400/D630 (using a 100-microsecond

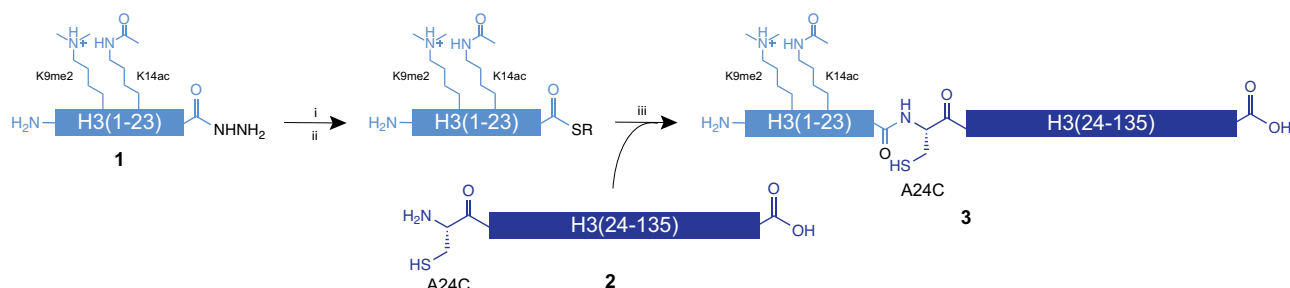


Fig. 5 | Semisynthesis of H3K9Me2K14Ac(A24C, C110A). H3K9Me2K14Ac(A24C, C110A), **3**, was generated via expressed protein ligation using peptide **1** and protein **2**. i) 0.2 M phosphate, 6 M Guanidine-HCl (GnCl), NaNO₂ (10 eq), pH 3.0–3.1, –15 °C, 15–20 min. ii) 4-mercaptophenylacetic acid (MPAA, 100 eq.), pH 6.8–7.0, room

temperature, R = phenylacetic acid. iii) Expressed protein ligation, 0.2 M phosphate, 6 M GnCl, MPAA, room temperature, 24 h. H histone, K lysine, me methyl, ac acetyl, A alanine, C cysteine.

Table 3 | Parameters used for TR-FRET displacement assays against seven methyl lysine reader proteins

Protein	Tracer ligand	Donor fluorophore	Acceptor fluorophore	Buffer
CBX2 (30 nM)	UNC4195 (30 nM)	10 nM Europium-W1024	2 nM and LANCE Ultra	20 mM Tris-HCl, 150 mM NaCl, 0.05%
CDYL2 (10 nM)	UNC4848 (10 nM)	10 nM Europium-W1024	ULight-anti6x-His	Tween-20 (v/v), and 2 mM DTT
MPP8 (5 nM)	P42 (20 nM)	10 nM Europium-W1024		
PHF1 (60 nM)	UNC6957 (90 nM)	10 nM Europium-W1024		
PHF19 (20 nM)	UNC6957 (40 nM)	10 nM Europium-W1024		
KDM7B (30 nM)	P3883 (50 nM)	10 nM Europium-W8044		
CHD1 (30 nM)	H3K4Me2-biotin (60 nM)	10 nM Europium-W1024		20 mM Tris-HCl, 75 mM NaCl, 0.05%
				Tween-20 (v/v), and 2 mM DTT

delay). TR-FRET output sign was expressed as emission ratios of acceptor/donor (665/615 nm) counts. Percent inhibition was calculated on a scale of 0% (i.e. activity with DMSO vehicle only) to 100% (100 μ M H3K9Me2K14Ac) using two full columns of control wells on each plate. The data was fitted with a four-parameter nonlinear regression analysis using ScreenAble to determine IC₅₀ values, plotted on GraphPad for visualization, and reported as an average of at least three technical replicates \pm s.d.

Kme reader selectivity evaluation. Similar protocols to those described above were used for the TR-FRET evaluation of the Kme reader selectivity of compounds using the parameters in Table 3.

Nucleosome TR-FRET displacement. The assay was run using white, low-volume, flat-bottom, nonbinding, 384-well microplates (Greiner, 784904) containing a total volume of 10 μ L per well. The buffer was made of 1X PBS pH 7.0, 0.005% Tween 20, and 2 mM DTT. Lance Europium (Eu)-W1024 Streptavidin conjugate (2 nM) and LANCE Ultra ULightTM-anti-6x-His antibody (50 nM) were used as donor and acceptor fluorophores associated with the tracer ligand and protein respectively. Final assay concentrations of 15 nM 6X histidine-tagged SETDB1 (residues 195–403, N-terminal tag) and 15 nM of H3K9Me2K14Ac-modified nucleosome were used for compound testing. A 10-point, three-fold serial dilution of each compound was tested as the primary hit validation. After addition, the plates were sealed with covers, mixed gently on a shaker for 1 min, centrifuged at 1000 \times g for 2 min, and allowed to equilibrate for 1 h in the dark. Plates were read with an EnVision 2103 Multilabel Plate Reader (PerkinElmer) using an excitation filter at 320 nm and emission filters at 615 and 655 nm. Emission signals (615 and 665 nm) were measured simultaneously using a dual mirror D400/D630 (using a 100-microsecond delay). TR-FRET output sign was expressed as emission ratios of acceptor/donor (665/615 nm) counts. Percent inhibition was calculated on a scale of 0% (i.e. activity with DMSO vehicle only) to 100%. The data was fitted with a four-parameter nonlinear regression analysis using GraphPad, where IC₅₀ values were

extracted after constraining the bottom to 0% and the top to 100%, and reported as an average of at least three technical replicates \pm s.d.

Isothermal titration calorimetry

ITC experiments were carried out at 10 °C on an Auto-ITC calorimeter (Malvern). Protein and peptide were kept in an identical buffer of 20 mM Tris/HCl [pH 7.0], 150 mM NaCl, and 2 mM TCEP. The final DMSO concentration was kept consistent throughout the cell and syringe. ITC experiments were carried out with protein and ligand concentrations of 100 μ M and 1.5 mM, respectively. Binding isotherms were analyzed by nonlinear least-squares fitting of the data using Microcal ORIGIN software (Microcal) using a one-site binding model and reported as an average of two technical replicates \pm s.d.

Radiometric methyltransferase activity evaluation

Dose-response evaluation. IC₅₀ values were determined for the compounds under the following conditions: For SETDB1, the assay used 2 nM SETDB1, 5 μ M SAM, and 100 nM biotinylated H3 1–25, with a 15-min incubation at 23 °C. For SETD2, the assay included 150 nM SETD2, 5 μ M SAM, and 1 μ M biotinylated H3 (21–44), with 20 μ L of reaction mixtures incubated for 1 h at 23 °C in buffer (20 mM Tris, pH 8.0; 0.01% Triton X-100; 5 mM DTT). The PRMT1 assay was performed as previously described²⁷.

Methyltransferase selectivity evaluation. The inhibitory effects of two compounds, UNC10013 and UNC10016, on the enzymatic activities of 33 epigenetic targets were examined using radioactivity-based activity assays as previously described²⁷.

MALDI-TOF-based methyltransferase activity assay

A catalytic assay was developed based on a previously described protocol by Basavapathruni et al.²⁸. The selected buffer was 20 mM bicine [pH 7.6], 0.002% Tween 20, and 1 mM DTT with the DTT being added fresh before use. The final conditions of reagents were as follows: 5 nM full-length SETDB1 (ActiveMotif), 1 μ M biotinylated H3 unmodified

peptide substrate (ARTKQTARKSTGGKAPRKQL-K(Biot)-NH₂, GenScript), and 20 μ M SAM. 384-well assay-ready plates were prepared with 10-point dose-response curves. For compound testing post-EpiG set screening, column 1 contained complete enzymatic inhibition by UNC00000421A at 100 μ M. Column 2 contained a 16-point, three-fold dilution dose-response curve of UNC00000421A starting at 200 μ M and going down the column. Columns 3–12 and 13–22 were used for compound dose-response curves. Column 23 was reserved for 2% DMSO only and Column 24 was a no enzyme control. Assay ready plates were centrifuged for 5 min at 1500 $\times g$. After centrifugation, 9 μ L of a mixture of SAM and SETDB1 was added using Multidrop Combi (ThermoFisher) to columns 1–23. 9 μ L of solution of SAM was added using a multi-channel pipette. The plate was incubated for 15 min in a dark cabinet before adding 1 μ L of the substrate to all columns using the MultiDrop Combi. The reactions were allowed to proceed for 1 h in a dark cabinet (not stacked). The reactions were quenched at 1 h with 1 μ L of 5% formic acid (0.5% final) using the MultiDrop Combi, mixed gently on a tabletop mixer for 1 min, and then centrifuged for 2 min at 1500 $\times g$. Plates were shipped for analysis by SAMDI Tech, Inc.

Fluorescence polarization

Fluorescence polarization (FP) experiments were conducted in black low-volume 384-well plates (Greiner Bio-One, US) with a final volume of 20 μ L per well. Each compound was serially diluted (12 or 16 concentrations) at 1.1X the tested concentrations in 18 μ L of an optimized buffer containing 20 mM Tris-HCl pH 8, 0.01% (v/v) Triton X-100, and 275 nM SETDB1 TTD (final concentration 250 nM in 20 μ L). The mixtures were preincubated at room temperature (\sim 25 $^{\circ}$ C) for 1 h, maintaining a final DMSO concentration of 2% or 4% in the assay. Following preincubation, 2 μ L of a 200 nM stock of 5' FITC-labeled H3K9Me2-K14Ac peptide in the optimized assay buffer was added to each well using a Multidrop Combi dispenser (Thermo Scientific), resulting in a final fluorescent peptide concentration of 20 nM. After a brief centrifugation at 300 $\times g$ (Eppendorf Centrifuge 5810R) for 5 min, the assay plates were covered to protect from light and incubated for 15 min at room temperature. The fluorescence polarization (FP) ratio was then measured using a BioTek Synergy H1 microplate reader (BioTek, Winooski, VT) with excitation at 485 nm and emission at 528 nm. The polarization values obtained were converted to percentage activity relative to the control with 100% activity and processed in GraphPad Prism using Sigmoidal, 4PL, X is log(concentration) fit with the bottom and top constrained to 0% and 100%, respectively. Each experiment was performed in triplicate, and the results were presented as the average and standard deviation of the three measurements.

Crystallography

Protein expression and purification. PCR amplified cDNA encoding SETDB1 TTD residues 197–403 was subcloned into the pET28-MHL vectors, downstream of the poly-histidine coding region. Following the transfection into *E. coli* BL21-CodonPlus-RIL, cultured cells were grown overnight at 37 $^{\circ}$ C in Terrific Broth supplemented with 50 μ g/mL Kanamycin and 35 μ g/mL chloramphenicol. SETDB1 TTD expression was induced by adding 1 mM IPTG (isopropyl-1-thio-D-galactopyranoside) and allowing overnight expression at 18 $^{\circ}$ C. The obtained culture was pelleted at low speed (7000 rpm for 10 min at 4 $^{\circ}$ C in a Beckman Coulter centrifuge). Harvested cells were resuspended (1 g of cell pellet per 10 mL) in the extraction buffer (20 mM HEPES pH 7.5, 500 mM NaCl, 2 mM TCEP, 5% glycerol) with protease inhibitor (0.1 mM phenylmethyl sulfonyl fluoride, PMSF). The cell suspension was supplemented with 5 μ L/L Benzonase Nuclease (in-house prepared) and sonicated for mechanical lysis on ice for 10 min total (10 s pulses with 7 s interruptions) (Sonicator 3000, Misoni). The crude extract was then clarified by high-speed centrifugation (60 min at 20,000 $\times g$ at 4 $^{\circ}$ C) in

a Beckman Coulter centrifuge to remove the cellular debris. Clarified lysate was first sent through the Hispur™ Ni-NTA resin (Thermo Scientific) column (\sim 20 mL bed volume for 60–70 g of the pellet) and eluted with 250 mM imidazole. Eluted fractions were passaged through Gel filtration HiLoad™ 26/600 Superdex (Cytiva) with 20 mM HEPES, pH 7.5, 250 mM NaCl, 0.5 mM TCEP, and 5% glycerol and further enriched with ion exchange Mono S HR 16/10 (SOURCE™ 30Q GE Healthcare) to 95% purity. Following the identification of SETDB1 TTD fractions on SDS-PAGE gels and confirmation of identity with LC-MS enriched fractions were pooled, concentrated to 7–8 mg/mL, snap-frozen, and stored at -80° C till use.

Crystallization and structural determination. SETDB1-UNC6535 structure was obtained by first generating Apo SETDB1-TTD crystals using 96-well vapor diffusion sitting drop plates by mixing equimolar amounts of protein and reservoir solution containing 20% (w/v) PEG8000, 0.2M Sodium Chloride, 0.1M Hepes, pH 7.5, 5% MPD. Apo crystals were then soaked with 5 mM UNC6535 ligand at room temperature for 2 h, then mounted by cryo-cooling in liquid nitrogen.

SETDB1-UNC10013 and SETDB1-UNC10016 structures were obtained by co-crystallization method. SETDB1-TTD protein, at 7 mg/mL (0.266 mM) was pre-incubated for 30 min at room temperature with 2.6 mM (10X times molar excess) of UNC10013 and UNC10016 compounds in the presence of 1:1000 ratio (trypsin: SETDB1 TTD) before crystallization. Co-crystallization of SETDB1-UNC10013 and SETDB1-UNC10016 were carried out in 96-well vapor diffusion sitting-drop plates by mixing 0.5 μ L of protein-compound mixture and 0.5 μ L of crystallization screen using Phoenix liquid dispensing robot (Art Robbins). Initial crystals were obtained after 72 h at 18 $^{\circ}$ C. After further optimization of the protein:compound ratio (2X times molar excess) and seeding, well-diffracting co-crystals of UNC10013 and UNC10016 were obtained in crystallization conditions containing 20% PEG 8000, 0.2 M NaCl, 0.1 M HEPES pH 7.5, 5% Ethyl Glycol, and 25% P3350, 0.1 M NH₄SO₄, 0.1 M Bis-Tris pH 6.5, respectively. Crystals were then cryo-cooled in liquid nitrogen. Dataset for SETDB1-UNC6535 was collected in-house using FRE Rigaku superbright. Datasets for SETDB1-UNC10013 and SETDB1-UNC10016 were collected at the CMCF-ID beamline (wavelength = 1.54 \AA) at the Canadian Light Source (CLS). Datasets were processed with HKL3000. Initial phases for SETDB1-UNC6535 was obtained by using (PDB ID: 5KE2) as initial model in Fourier transform with Refmac. Initial phases for SETDB1-UNC10013 and SETDB1-UNC10016 were obtained by using (PDB ID: 3DLM) as initial model in PHASER for molecular replacement. Model building was performed in COOT and the structure was validated with Molprobity. Ligand restraints were generated using Grade Web Server (<http://grade.globalphasing.org>).

MALDI-TOF

Initial assessment of covalent bond formation. The buffer was made of 25 mM Tris/HCl, 50 mM NaCl (pH 7.5). Experiments were carried out using 98 μ L of SETDB1-3TD (residues 195–403, N-terminal 6X His tag) protein and 2 μ L of compound for final concentrations of 10 μ M of protein and 100 μ M of compound with a 2% final DMSO concentration. After 2 h of incubation at room temperature, 1 μ L of the mixture and 1 μ L of α -cyano-4-hydroxycinnamic acid (CHCA) MALDI matrix were spotted on a MALDI sample plate. Each spot was analyzed by MALDI-TOF on an AB Sciex 5800 MALDI-TOF/TOF instrument using the linear mode. Data is visualized using mMass version 5.5.0 with normalized intensities, baseline corrections (precision: 15, relative offset: 25) and smoothing (window size: 30 m/z, 5 cycles). Three biological replicates were obtained for each condition ($n = 3$).

Qualitative reactivity comparison. A similar protocol than described above was used except that the final concentrations of protein and compound were set at 10 μ M and the mixture was incubated on ice. At

the desired time point, an 8 μL sample was quenched by adding 2 μL of 5% TFA aqueous solution (v/v) before being spotted.

Intrinsic reactivity evaluation with glutathione

The protocol was adapted from Resnick et al.²⁹. Briefly, 500 μM of compound was incubated with 2.5 mM of glutathione and 800 μM of Rhodamine B, used an internal standard, in 100 mM potassium phosphate buffer (pH 7.4) and MeCN (9:1 ratio respectively). Every hour, for up to 8 h, 6 μL were analyzed on the LC-MS instrument. LC-MS data for all compounds was acquired using an Agilent 6110 Series system with the UV detector set to 254 nm. Samples were injected (<10 μL) onto an Agilent Eclipse Plus 4.6 \times 50 mm, 1.8 μm , C18 column at room temperature. Mobile phases A (H₂O + 0.1% acetic acid) and B (MeCN + 1% H₂O + 0.1% acetic acid) were used with a linear gradient from 10% to 100% B in 5.0 min, followed by a flush at 100% B for another 2 min with a flow rate of 1.0 mL/min. Mass spectra (MS) data were acquired in positive ion mode using an Agilent 6110 single quadrupole mass spectrometer with an electrospray ionization (ESI) source. The % unreacted compound was calculated by normalizing the area under curve ratio of the compound to Rhodamine B. The resulting % unreacted compound was plotted in function of time and the data was fitted with a one-phase decay regression analysis using GraphPad providing the $t_{1/2}$ values.

Intact protein mass spectrometry

40 μM of 3TD protein was incubated with 400 μM of compound in 25 mM HEPES pH 7.5, 300 mM NaCl for a total volume of 20 μL . The sample was incubated overnight at 4 °C before undergoing sample preparation for mass spectrometry.

Samples were diluted to a concentration of 0.5 $\mu\text{g}/\mu\text{L}$ in peptide background electrolyte (BGE). Samples were injected onto an HR Chip (908Devices Inc.) using a ZipChip system (908Devices Inc.) interfaced to a Thermo QExactive HF Biopharma mass spectrometer. The MS data was acquired through Tune (Thermo, v. 2.9) and settings included: scan range 500–2000 m/z, in-source CID 15 eV, mass resolution 15,000, 3 microscans, 10 ms maximum injection time. The ZipChip settings included: field strength 500 V/cm, injection volume 1 nL, pressure assist start time 0.5 min, analysis run time 3.5 min. Intact mass spectra were deconvoluted using PMI Intact Mass software (Protein Metrics Inc. v5.1.1). Provided sequences were used to assign peaks in Byos. Threshold for protein assignment = \pm 5 Da. Relative abundance was calculated by dividing the intensity of a given peak by the max peak intensity. Each sample was analyzed as a single independent experiment ($n = 1$).

Liquid chromatography coupled to tandem mass spectrometry (LC-MS/MS)

The same samples used above were diluted to 50 μL with 2 M urea. Samples were reduced with 5 mM DTT at 37 °C for 45 min, then alkylated with 15 mM iodoacetamide at room temperature in the dark for 45 min. The samples were diluted to 1 M urea and subjected to digestion with trypsin (Promega) overnight at 37 °C at a 1:20 enzyme: protein ratio. The resulting peptide samples were acidified to 0.5% TFA, desalted using C18 Desalting Spin Columns (Thermo), then the eluates were dried via vacuum centrifugation. The samples were reconstituted in a 2% ACN, 0.1% formic acid solution prior to LC-MS/MS analysis.

Samples were analyzed in technical duplicate by LC-MS/MS using a Thermo Easy nLC 1200 – QExactive HF Mass Spectrometer ($n = 2$). Samples were injected onto an Easy Spray PepMap C18 column (75 μm id \times 25 cm, 2 μm particle size) (Thermo Scientific) and separated over a 45 min method. The gradient for separation consisted of 5–38% mobile phase B at a 250 nL/min flow rate, where mobile phase A was 0.1% formic acid in water and mobile phase B consisted of 0.1% formic acid in 80% ACN. The QExactive HF was operated in data-dependent acquisition mode (DDA) where the 15 most intense precursors were selected for

subsequent fragmentation. Resolution for the precursor scan (m/z 350–1600) was set to 60,000 with a target value of 3×10^6 ions, 100 ms max injection time. MS/MS scans resolution was set to 15,000 with a target value of 5×10^4 ions, 60 ms max injection time. The normalized collision energy was set to 27% for HCD. Dynamic exclusion was set to 30 s, peptide match was set to preferred, and precursors with unknown charge or a charge state of 1 and ≥ 7 were excluded.

Raw data were analyzed using Proteome Discoverer 2.5 (Thermo Scientific). The samples were searched against the Recombinant 3TD protein sequence, along with an E. coli database from Uniprot (UP000000625; containing 4448 protein sequences). A common contaminants database was appended to the reference proteome. Parameters used in PD included: precursor ion tolerance – 20 ppm; product ion tolerance – 20 ppm; enzyme specificity, set to trypsin, up to two missed cleavages were allowed. Variable modifications: methionine oxidation, cysteine carbamidomethylation, compound covalent modification.

k_{inact}/K_i measurement using mass dilution SETDB1 3TD TR-FRET

Mass dilution TR-FRET assays were run using the white, high volume, flat-bottom, nonbinding, 384-well OptiPlate™ from PerkinElmer (Part No. 6007290) containing a total assay volume of 100 μL per well. All experiments were run at room temperature with the same buffer composition and final concentrations of protein and FRET reagents as the TR-FRET methods described above. The test compounds and SETDB1 3TD protein were diluted in Eppendorf tubes for incubation at the desired testing concentrations (2.5X). In the OptiPlate, the remaining components necessary for the FRET assay were dispensed at 60 μL (1.67X) per well in preparation for mass dilution. Starting at time point zero, 40 μL aliquots of the protein-peptide stock were transferred from the Eppendorf tube to the Optiplate for mass dilution every three minutes for 30 min total (11 total wells per concentration, 100 μL total). The dilution factors were predetermined so the mass dilution step reduces the peptide concentration below the reported IC₅₀. All TR-FRET components are diluted to the final concentrations listed in the TR-FRET methods above (1X). A DMSO control sample was also included for data normalization at each time point tested. 100% (saturated with known inhibitor) and 0% (no inhibitor present) inhibition controls were incorporated to calculate the percentage of inhibition for all data points. Following mass dilution, each time point was incubated for 15 min to allow for any reversible compound binding to be diluted off. Then, each data point was read on an EnVision 2103 Multilabel Plate Reader (PerkinElmer) using a 320 nm excitation filter and 615 and 665 nm emission filters. Emission signals were measured simultaneously using a dual mirror D400/D630 and 100 μsec delay. The TR-FRET output signal was expressed as a ratio of acceptor/donor (665 nm/615 nm) emission counts. The normalized percent inhibition for each concentration tested was plotted at each time point. The data was fitted using a linear fit, and the slope (k_{obs}) of each concentration was plotted against the different peptide concentrations tested. From this, the max k_{obs} from these experiments is taken as the k_{inact} , while the concentration at which $1/2 k_{\text{inact}}$ is observed is taken as the K_i . From here, the inactivation efficiency can be calculated using k_{inact}/K_i . GraphPad Prism 9.0 was used for data visualization, fitting, and figure preparation.

Differential scanning fluorimetry

DSF assays were performed using AB ViiA 7 Real-Time PCR System. The buffer was made of 20 mM HEPES, 200 mM NaCl, pH 7.5. Experiments were carried out using 8 μL of SETDB1-3TD (residues 196–403, N-terminal His tag) and 20X concentration Sypro Orange dye (5000X DMSO stock, ThermoFisher) and 2 μL of ligand for a final concentration of 20 μM of protein and 200 μM of ligand with 1.1% of DMSO. Plates were incubated for 15 min before running the temperature gradient (1 °C/min, from 25 to 90 °C). Values are presented as an

average of at least two replicates \pm s.d. calculated using the Boltzmann method from the Protein Thermal Shift software (ThermoFisher).

Cell culture and transfection

MCF-7 cells were obtained from the UNC Lineberger Tissue Culture facility and were cultured in DMEM (Sigma or Corning) supplemented with 10% FBS, 100 U/mL penicillin, 100 μ g/mL streptomycin (Sigma), 0.01 mg/mL of insulin from bovine pancreas (Sigma), with (Cell Titer Glo assay) or without (ABPP experiment) 1X Minimum Essential Medium Non-Essential Amino Acids Solution (Gibco). Cells were grown and maintained in 10 cm-diameter tissue culture dishes in an incubator at 37 °C with 5% CO₂.

Human cervical cancer cell line HeLa was purchased from ATCC and cultured in DMEM medium supplemented with 10% FBS, 100 Units/mL penicillin and 100 mg/mL streptomycin. Cell transfection was performed using polyethylenimine (23866-1, Polysciences, Inc) according to manufacturer instructions.

Cysteine-targeted activity-based protein profiling

In-lysate reactive cysteine profiling. The streamlined reactive cysteine profiling was performed as described in previous work^{30,31}. To briefly describe the process, the native and soluble proteome of MCF-7 cells was generated through homogenization by sonication (5 min, 3-s on, 5-s off, 50% amplitude) in native lysis buffer (PBS, pH 7.4, 0.1% NP-40) on ice. To profile reactive cysteine, 30 μ g of lysate (2 μ g/ μ L, spiked with recombinant SETDB1 at 0.5% w/w of the total proteome) in 15 μ L of lysis buffer was loaded into a 96-well plate. The lysate was treated sequentially with 10 μ M of the compound and 500 μ M of the DBIA probe for 1 h respectively at room temperature. The reaction was quenched by adding 3 μ L of a 1:1 mixture of SP3 beads (50 mg/mL, Cat. #45152105050250 and Cat. #65152105050250) and 30 μ L of ~98% ethanol containing 20 mM DTT. After a 15-min incubation, the plate was placed on a magnetic stand, and the liquid was aspirated. The beads were washed once with 200 μ L of 80% ethanol, resuspended in 25 μ L of lysis buffer containing 20 mM IAA, incubated in the dark for 30 min with vigorous shaking, and then 50 μ L of ~98% ethanol containing 20 mM DTT was added. After another 15-min incubation, the beads were washed twice with 80% ethanol. The remaining beads were resuspended in 30 μ L of 200 mM EPPS buffer (pH 8.5) containing 0.3 μ g of Lys-C and 0.3 μ g of trypsin and incubated at 37 °C overnight. The next day, 60 μ g of TMT reagent was added to the mixture of digested peptides and beads to achieve a final acetonitrile concentration of ~30%, followed by gentle mixing at room temperature for 60 min and quenching with 7 μ L of 5% hydroxylamine. All TMT-labeled samples were combined, dried using a SpeedVac, and desalted using a 100-mg Sep-Pak column. The labeled peptides were enriched using 80 μ L of Pierce™ High-capacity Streptavidin Agarose (Cat. #20359) in 100 mM HEPES buffer (pH 7.4) for 3 h at room temperature. The remaining agarose resin was washed sequentially with 300 μ L of 100 mM HEPES (pH 7.4) with 0.05% NP-40 twice, 350 μ L of 100 mM HEPES (pH 7.4) three times, and 400 μ L of water once on an Ultrafree-MC centrifugal filter (hydrophilic PTFE, 0.22 μ m pore size). The peptides were eluted sequentially with elution buffer (80% acetonitrile, 0.1% formic acid) twice and elution buffer at 72 °C once. The combined eluate was dried, desalted via StageTip, and resuspended in loading buffer (5% ACN and 5% FA) prior to LC-MS analysis.

LC-FAIMS-MS/MS analysis. Enriched cysteines were loaded onto a 100- μ m capillary column packed with 25 cm of Accucore 150 resin (2.6 μ m, 150 Å; Thermo Fisher Scientific) and separated using a 180-min method on a NanoLC-1200 UPLC system. Cysteine data were collected using a high-resolution MS/MS method on an Orbitrap Eclipse mass spectrometer coupled with a FAIMS Pro device. Each cysteine sample was analyzed twice with different sets of FAIMS compensation voltages (CVs): 1) -60, -45, and -35V, and 2) -70, -55, and -30V. MS1 scans were

collected in the Orbitrap with 60 K resolution, a 400–1600 m/z scan range, standard AGC, and a 50 ms maximum injection time (IT). Data-dependent MS2 scans were acquired in Top Speed mode with a cycle time of 1 s, selecting and fragmenting precursors using 36% HCD. MS2 scans were collected in the Orbitrap with 50 K resolution, a fixed 110–2000 m/z scan range, 500% AGC, and a maximum IT of 86 ms. Dynamic exclusion was set to 120 s with a mass tolerance of \pm 10 ppm. The flowthrough was analyzed using a 60-min LC-FAIMS-MS/MS in data-dependent analysis, similar to the settings used for analyzing cysteine samples.

Data analysis for cysteine identification, localization, and quantification.

Raw files were searched using the Comet search engine (ver. 2019.01.5)³² with the Uniprot human proteome database (downloaded 11/24/2021). The settings included a 50 ppm precursor error tolerance, a 0.9 Da fragment error tolerance, and peptide modifications such as fixed Cys carboxyamidomethylation (+57.0215), fixed Lys/N-terminal TMTpro (+304.2071), variable Met oxidation (+15.9949), and variable Cys DBIA mass shift (+239.1628) based on carboxyamidomethylation. Peptide spectral matches were filtered to a peptide false discovery rate (FDR) of <1% using linear discriminant analysis and then filtered to obtain a 1% protein FDR at the entire dataset level employing a target-decoy strategy^{33,34}. Cysteine-modified peptides were then filtered for site localization using the AScorePro algorithm with a cutoff of 13 ($P < 0.05$) as previously described³⁵. Unique peptides and unique cysteine sites were summarized from all peptide spectral matches (PSMs) and reported. For TMT reporter quantification, a total sum signal-to-noise ratio of all reporter ions of 180 was required, with fewer than three missing values. Peptide and cysteine site quantitative values were normalized based on sample loading differences obtained from analyzing the flowthrough sample.

Cell titer Glo proliferation evaluation

5000 MCF-7 cells in 25 μ L of media were seeded in each well of a 384-well white tissue culture-treated plate (Corning #3570). After 24 h, the media was replaced with media containing the desired compound concentration to obtain a dose-response. Treated cells were then incubated for 24 h, 48 h, or 72 h at 37 °C. Cell proliferation analysis was performed using the Cell Titer Glo Kit (G9241, Promega) according to the manufacturer's instructions. Luminescent signals were measured using the Promega GloMax Plate Reader with an integration time of 0.3 s per well. Percent viability was calculated as a percentage of the related DMSO-treated cells.

Caco-2 cell permeability evaluation

The Caco-2 cell permeability evaluation data was obtained from the In vitro ADME laboratory at Pharmaron (Beijing, China).

Cellular thermal shift assay

SETDB1 (3TD, 197–403aa) was cloned into pBIT3.1-N (Promega, #N2361) and pBIT3.1-C (Promega, #N2371) plasmids. HEK293T cells were plated in 6-well plates (1e6/well) and reversely transfected with 0.2 μ g HiBIT -tagged SETDB1 (3TD) and 1.8 μ g of empty plasmid using X-tremeGene XP transfection reagent (Roche), following manufacturer's instructions. The next day cells were trypsinized and resuspended in OptiMEM (no phenol red, Gibco) at density 2e5/ml. After compound or DMSO addition (the same DMSO concentration in each sample) cells were transferred to 96-well pcr plates (40 μ L/well), incubated for 1 h at 37 °C and heated for 3 min. For permeabilized CETSA cells were incubated in the presence of digitonin (50 μ g/ml) for 20 min at RT. After 3 min, 40 μ L of LgBIT solution (200 nM LgBIT, 2% NP-40, protease inhibitors in OptiMEM no phenol red) was added and incubated at RT for 10 min. Next, 20 μ L of NanoGlo substrate (8 μ g/ml, Promega) was added, mixed gently and 20 μ L was transferred to 384 white plates in triplicates and the bioluminescence

signal was read in the ClarioStar plate reader. The results and mean \pm s.d.

Cellular Akt methylation and phosphorylation evaluation

Plasmid construction. pcDNA3-HA-Akt1 was constructed by cloning corresponding PCR fragments into pcDNA3-HA vector by BamHI and SalI sites.

Akt1-BamHI-Forward: 5'-GCATGGATCCAGCGACGTGGCTATT GTG-3'

Akt1-SalI-Reverse: 5'-GCATGTCGACTCAGGCCGTGCCGCTGGC-3'

Antibodies. All antibodies were used at a 1:1000 dilution in TBST buffer with 5% non-fat milk for western blotting unless specified. Anti-HA-Tag antibody (3724), anti-Tri-Methyl Lysine motif antibody (14680) and Anti-phospho-Akt-Thr308 antibody (9275) were obtained from Cell Signaling Technology. Ant-Vinculin antibody (sc-25336) was purchased from Santa Cruz Biotechnology.

Immunoblot and immunoprecipitations analyses. Cells were lysed in EBC buffer (50 mM Tris pH 7.5, 120 mM NaCl, 0.5% NP-40) or Triton X-100 buffer (50 mM Tris, pH 7.5, 150 mM NaCl, 1% Triton X-100) supplemented with protease inhibitor cocktail and phosphatase inhibitor cocktail. The protein concentrations of whole cell lysates were measured by NanoDrop OneC using the Bio-Rad protein assay reagent. Equal amounts of whole cell lysates were loaded by SDS-PAGE and immunoblotted with indicated antibodies. For immunoprecipitations analysis, 1 mg total lysates were incubated with the anti-HA agarose beads (A-2095, Sigma) for 3–4 h at 4 °C. The recovered immunocomplexes were washed three times with NETN buffer (20 mM Tris, pH 8.0, 100 mM NaCl, 1 mM EDTA and 0.5% NP-40) before being resolved by SDS-PAGE and immunoblotted with indicated antibodies.

Reporting summary

Further information on research design is available in the Nature Portfolio Reporting Summary linked to this article.

Data availability

The authors declare that the data supporting the findings of this study are available within the paper and its Supplementary Information files. Source Data are provided with this paper. Should any raw data files be needed in another format they are available from the corresponding author upon request. Crystallographic data for the structures reported in this article have been deposited at the Protein Data Bank with PDB ID: [8GSE](#), [9CUW](#), [9CUX](#). The mass spectrometry proteomics data have been deposited to ProteomeXchange with accession code [PXD056190](#) and [PXD056206](#). Source data are provided with this paper.

References

- Martin, C. & Zhang, Y. The diverse functions of histone lysine methylation. *Nat. Rev. Mol. Cell Biol.* **6**, 838–849 (2005).
- Black, J. C., Van Rechem, C. & Whetstone, J. R. Histone Lysine Methylation Dynamics: Establishment, Regulation, and Biological Impact. *Mol. Cell* **48**, 491–507 (2012).
- Musselman, C. A., Khorasanizadeh, S. & Kutateladze, T. G. Towards understanding methyllysine readout. *Biochim. Biophys. Acta Gene Regul. Mechan.* **1839**, 686–693 (2014).
- Zhao, S., Allis, C. D. & Wang, G. G. The language of chromatin modification in human cancers. *Nat. Rev. Cancer* **21**, 413–430 (2021).
- Park, I.-G., Jeon, M., Kim, H. & Lee, J. M. Coordinated methyl readers: Functional communications in cancer. *Semin Cancer Biol.* **33**, 88–99 (2022).
- Jurkowska, R. Z. et al. H3K14ac is linked to methylation of H3K9 by the triple Tudor domain of SETDB1. *Nat. Commun.* **8**, 2057 (2017).
- Schultz, D. C., Ayyanathan, K., Negorev, D., Maul, G. G. & Rauscher, F. J. SETDB1: A novel KAP-1-associated histone H3, lysine 9-specific methyltransferase that contributes to HP1-mediated silencing of euchromatic genes by KRAB zinc-finger proteins. *Genes Dev.* **16**, 919–932 (2002).
- Fei, Q. et al. Histone methyltransferase SETDB1 regulates liver cancer cell growth through methylation of p53. *Nat. Commun.* **6**, 8651 (2015).
- Wang, G. et al. SETDB1-mediated methylation of Akt promotes its K63-linked ubiquitination and activation leading to tumorigenesis. *Nat. Cell Biol.* **21**, 214–225 (2019).
- Guo, J. et al. AKT methylation by SETDB1 promotes AKT kinase activity and oncogenic functions. *Nat. Cell Biol.* **21**, 226–237 (2019).
- She, X. et al. SETDB1 Methylates MCT1 Promoting Tumor Progression by Enhancing the Lactate Shuttle. *Adv. Sci.* **10**, 2301871 (2023).
- Guo, Y. et al. Structure-Guided Discovery of a Potent and Selective Cell-Active Inhibitor of SETDB1 Tudor Domain. *Angew. Chem. Int. Ed.* **60**, 8760–8765 (2021).
- Uguen, M. et al. SETDB1 Triple Tudor Domain Ligand, (R,R)-59, Promotes Methylation of Akt1 in Cells. *ACS Chem. Biol.* **18**, 1846–1853 (2023).
- Ackloo, S. et al. A Target Class Ligandability Evaluation of WD40 Repeat-Containing Proteins. *J. Med. Chem.* <https://doi.org/10.1021/ACS.JMEDCHEM.4C02010> (2024).
- Martin, J. S., Mackenzie, C. J., Fletcher, D. & Gilbert, I. H. Characterising covalent warhead reactivity. <https://doi.org/10.1016/j.bmc.2019.04.002> (2019).
- Schwartz, P. A. et al. Covalent EGFR inhibitor analysis reveals importance of reversible interactions to potency and mechanisms of drug resistance. *Proc. Natl Acad. Sci. USA* **111**, 173–178 (2014).
- Wesley, N. A. et al. Time Resolved-Fluorescence Resonance Energy Transfer platform for quantitative nucleosome binding and footprinting. *Protein Sci.* **31**, e4339 (2022).
- Hartung, I. V., Rudolph, J., Mader, M. M., Mulder, M. P. C. & Workman, P. Expanding Chemical Probe Space: Quality Criteria for Covalent and Degradable Probes. *J. Med. Chem.* **66**, 9297–9312 (2023).
- Rectenwald, J. M. et al. A General TR-FRET Assay Platform for High-Throughput Screening and Characterizing Inhibitors of Methyl-Lysine Reader Proteins. *SLAS Discov.* **24**, 693–700 (2019).
- Strelow, J. M. A Perspective on the Kinetics of Covalent and Irreversible Inhibition. *SLAS Discov.* **22**, 3–20 (2017).
- Ma, T. et al. SETDB1: Progress and prospects in cancer treatment potential and inhibitor research. *Bioorg. Chem.* **145**, 107219 (2024).
- Hassanie, H. et al. SETDB1 as a cancer target: challenges and perspectives in drug design. *RSC Med. Chem.* **15**, 1424–1451 (2024).
- Luger, K., Rechsteiner, T. J. & Richmond, T. J. Preparation of nucleosome core particle from recombinant histones. *Methods Enzymol.* **304**, 3–19 (1999).
- Zheng, J. S., Tang, S., Qi, Y. K., Wang, Z. P. & Liu, L. Chemical synthesis of proteins using peptide hydrazides as thioester surrogates. *Nat. Protoc.* **8**, 2483–2495 (2013).
- Skrajina, A. et al. Comprehensive nucleosome interactome screen establishes fundamental principles of nucleosome binding. *Nucleic Acids Res.* **48**, 9415–9432 (2020).
- Lowary, P. T. & Widom, J. New DNA sequence rules for high affinity binding to histone octamer and sequence-directed nucleosome positioning. *J. Mol. Biol.* **276**, 19–42 (1998).
- Bhattacharya, D. et al. Development of selective class I protein arginine methyltransferase inhibitors through fragment-based drug design approach. *Eur. J. Med. Chem.* **260**, 115713 (2023).
- Basavapathruni, A. et al. Characterization of the Enzymatic Activity of SETDB1 and Its 1:1 Complex with ATF7IP. *Biochemistry* **55**, 1645–1651 (2016).

29. Resnick, E. et al. Rapid Covalent-Probe Discovery by Electrophile-Fragment Screening. *J. Am. Chem. Soc.* **141**, 8951–8968 (2019).
30. Kuljanin, M. et al. Reimagining high-throughput profiling of reactive cysteines for cell-based screening of large electrophile libraries. *Nat. Biotechnol.* **39**, 630 (2021).
31. Yang, K. et al. Accelerating multiplexed profiling of protein-ligand interactions: High-throughput plate-based reactive cysteine profiling with minimal input. *Cell Chem. Biol.* **31**, 565–576.e4 (2024).
32. Eng, J. K., Jahan, T. A. & Hoopmann, M. R. Comet: An open-source MS/MS sequence database search tool. *Proteomics* **13**, 22–24 (2013).
33. Elias, J. E. & Gygi, S. P. Target-decoy search strategy for increased confidence in large-scale protein identifications by mass spectrometry. *Nat. Methods* **4**, 207–214 (2007).
34. Savitski, M. M., Wilhelm, M., Hahne, H., Kuster, B. & Bantscheff, M. A scalable approach for protein false discovery rate estimation in large proteomic data sets. *Mol. Cell. Proteom.* **14**, 2394–2404 (2015).
35. Gassaway, B. M. et al. A multi-purpose, regenerable, proteome-scale, human phosphoserine resource for phosphoproteomics. *Nat. Methods* **19**, 1371–1375 (2022).

Acknowledgements

This work was supported by the PhRMA Foundation (Drug Discovery postdoctoral fellowship) to M.U. and the National Institute of General Medical Sciences, NIH (grant R35GM139514) to S.V.F. This work was also supported by the National Cancer Institute of the National Institutes of Health under award number P30CA016086. The content is solely the responsibility of the authors and does not necessarily represent the official views of the National Institutes of Health. The authors thank Juanita Rubiano Sánchez and Tiffany Peters for reviewing the experimental chemistry and biology data. The authors thank B. Hardy for assembling the screening plate for TR-FRET. Part or all of the research described in this paper was performed using beamline CMCF-ID at the Canadian Light Source, a national research facility of the University of Saskatchewan, which is supported by the Canada Foundation for Innovation (CFI), the Natural Sciences and Engineering Research Council (NSERC), the National Research Council (NRC), the Canadian Institutes of Health Research (CIHR), the Government of Saskatchewan, and the University of Saskatchewan. The Structural Genomics Consortium provides support to authors at the University of Toronto (M.S., F.L., M.M.S., S.B., C.H.A., S.A., D.B.-L., L.H.) and is a registered charity (no. 1097737) that receives funds from Bayer AG, Boehringer Ingelheim, Bristol Myers Squibb, Genentech, Genome Canada through Ontario Genomics Institute [OGI-196], EU/EFPIA/OICR/McGill/KTH/Diamond Innovative Medicines Initiative 2 Joint Undertaking [EUbOPEN grant 875510], Janssen, Merck KGaA (aka EMD in Canada and US), Pfizer, and Takeda.

Author contributions

Conceptualization: M.U., S.V.F.; Investigation and analysis: M.U., D.J.S., M.S., Y.D., F.L., M.M.S., K.Y., Y.Z., M.A.S., J.L.N., J.M.W., S.B., J.M.R., A.L.M., T.S.W.; Supervision: L.E.H., C.H.A., S.A., S.P.G., R.K.M., D.B., P.L., L.H., L.I.J., K.H.P., S.V.F.; Resources and funding acquisition: L.E.H., C.H.A., S.P.G., R.K.M., D.B., P.L., L.H., L.I.J., K.H.P., S.V.F.; Writing – Original draft: M.U., S.V.F.; Writing – Review and Editing: M.U.; D.J.S., F.L., M.M.S., K.Y., L.E.H., S.A., R.K.M., D.B., P.L., L.H., L.I.J., K.H.P., S.V.F.

Competing interests

The authors declare no competing interests.

Additional information

Supplementary information The online version contains supplementary material available at <https://doi.org/10.1038/s41467-025-57005-3>.

Correspondence and requests for materials should be addressed to Stephen V. Frye.

Peer review information *Nature Communications* thanks Stephen Antonyamy, Gianluca Sbardella and the other anonymous, reviewer(s) for their contribution to the peer review of this work. A peer review file is available.

Reprints and permissions information is available at <http://www.nature.com/reprints>

Publisher's note Springer Nature remains neutral with regard to jurisdictional claims in published maps and institutional affiliations.

Open Access This article is licensed under a Creative Commons Attribution-NonCommercial-NoDerivatives 4.0 International License, which permits any non-commercial use, sharing, distribution and reproduction in any medium or format, as long as you give appropriate credit to the original author(s) and the source, provide a link to the Creative Commons licence, and indicate if you modified the licensed material. You do not have permission under this licence to share adapted material derived from this article or parts of it. The images or other third party material in this article are included in the article's Creative Commons licence, unless indicated otherwise in a credit line to the material. If material is not included in the article's Creative Commons licence and your intended use is not permitted by statutory regulation or exceeds the permitted use, you will need to obtain permission directly from the copyright holder. To view a copy of this licence, visit <http://creativecommons.org/licenses/by-nc-nd/4.0/>.

© The Author(s) 2025